Electrical Power and Energy Systems 126 (2021) 106413

Contents lists available at ScienceDirect

Electrical Power and Energy Systems

journal homepage: www.elsevier.com/locate/ijepes

A generalized approach for design of contingency versatile DC voltage droop control in multi-terminal HVDC networks

Sawsan S. Sayed*, Ahmed M. Massoud

Department of Electrical Engineering, Qatar University, P.O. Box: 2713, Doha Qatar

ARTICLE INFO

Keywords:
DC grid
Adaptive droop control
DC power flow
Droop gains
MTDC

ABSTRACT

The non-deterministic nature of power fluctuations in renewable energy sources impose challenges to the design of DC voltage-droop controller in Multi-Terminal High-Voltage DC (MTDC) systems. Fixed droop control does not consider converters' capacity and system operational constraints. Consequently, an adaptive droop controller is counseled for appropriate power demand distribution. The previous adaptive droop control studies based on the converters' Available-Headroom (AH) have lacked the demonstration of the droop gain design during consecutive power disturbances. In this paper, the design of the adaptive DC voltage droop control is investigated with several approaches, based on the permitted converters' global and/or local AH and Loading Factor (LF). Modified adaptive droop control approaches are presented along with a droop gain perturbation technique to achieve the power-sharing based on the converters' AH and LF. In addition, the impact of Multi-Updated (MU), Single-Updated (SU), and Irregular-Updated (IU) droop gains is investigated. The main objective of the adaptive droop control design is to minimize the power-sharing burden on converters during power variations/consecutive disturbances while maintaining the constraints of the DC grid (i.e., voltage and power rating). The presented approaches are evaluated through case studies with a 4-terminal and 5-terminal radial MTDC networks.

1. Introduction

Point-to-point High-Voltage Direct Current (HVDC) transmission system has been overruled by the development of Multi-Terminal HVDC (MTDC) transmission network due to its capabilities to provide alternative flow paths, multi-regional interconnections for better balance service, and reduced influence of diversified power generation portfolios (i.e., wind source intermittent variations) [1–5].

The essential indicator for the power balance between the sending and receiving terminals in an MTDC system is the terminals' DC voltages [6,7]. The limited inertia and stored energy in DC systems (i.e., available merely in the capacitors of the converters) make the network DC voltages susceptible to fast changes [8,9]. Regardless of the absence of universal grid codes for the MTDC systems, in general, a secure MTDC network operation requires the nodes' DC voltages to be within 5% to 10% of the nominal voltage level. Otherwise, over-voltage may cause infrastructure damage, while under-voltage may introduce dis-oriented control actions for the converters [7,10].

1.1. DC voltage control

The conventional classification of the DC voltage control in MTDC systems can be divided into non-distributed control (i.e., master–slave where the single slack converter is responsible for the voltage control), and distributed control (i.e., multiple converters share the voltage control such as voltage margin control and DC voltage droop control) [11,12]. The DC voltage droop control has been introduced as a proper approach to DC voltage control, along with reducing the dependence on communication among converters [11,12].

The DC voltage droop control in an MTDC network can be achieved via a centralized controller and/or a decentralized controller [10,13,14,15]. The operation of the droop control through the hierarchical control layers can attain multiple optimization objectives (e.g., grid loss minimization, voltage and power management, and market/economic-based power dispatch) [9,13,16–20]. However, this requires fast communication among the Voltage Source Converters (VSCs) across the network [13]. While the decentralized control can be achieved with less communication requirement by a fixed droop control [17,21–24], or by an adaptive droop control [25–29]. The stochastic power generation during normal operation, in addition to the

* Corresponding author.
E-mail addresses: ssayed@qu.edu.qa (S.S. Sayed), ahmed.massoud@qu.edu.qa (A.M. Massoud).

https://doi.org/10.1016/j.ijepes.2020.106413
Received 10 April 2020; Received in revised form 2 July 2020; Accepted 30 July 2020
Available online 24 November 2020

Nomenclature

V	DC voltage.
I	DC current.
P	DC power.
K	Droop gain.
R	DC transmission line resistance.
MU Ks	Multi-updated droop gains.
SU Ks	Single-updated droop gains.
IU Ks	Irregular-updated droop gains.

Subscripts

wi	i^{th} WSC.
gj	j^{th} GSC.
gj,r	Rating of the j^{th} GSC.
gL	No-load DC voltage.
max	Maximum value.
min	Minimum value.

unpredicted disturbance operation, as a converter or line outage, may cause power-imbalance sharing among the converters without insight into the converters' loading capability [12]. Fixed droop control can be designed for a specific range of operation concerning the power rating of the converter. However, the actual loading and capacity margin of the converters are not considered [12]. Moreover, sub-optimal power flow can be achieved with a fixed droop constant for the objective of transmission loss minimization, as has been introduced in [22]. Nevertheless, the consideration of the actual converter loading for significant power variations is vital for MTDC system stability. The impact of unforced and forced MTDC system parameters variations, including fixed droop control, has been elaborated in [18,19], and [24].

1.2. Adaptive DC voltage droop control

To avoid the problems introduced by the fixed DC voltage droop control, several types of adaptive DC voltage droop control have been proposed. In [9], a local control approach for DC voltage control has been proposed for the MTDC network based on forecasting the optimal characteristics of VSCs a-day-ahead to manage the power imbalance in case of intermittent power production from the wind farms. Nonetheless, the impact of the forecasting uncertainty on the droop gains design needs careful study. In [25], an autonomous adaptive droop control has been proposed for power-sharing based on the converters' local Available Headroom (AH) in case of a converter outage event. The droop coefficients are calculated offline regularly, to reduce the power-sharing burden for converters operating near their limits to evade possible overloading. However, this model is operating-point dependent. This issue will be further elaborated in this paper. The previous work has been supported by a dynamic stability study approach for Alternating Current (AC) grid stability with adaptive droop control [30]. In [26], to support the voltage stability of weak AC grids, adaptive droop control has been introduced to share the power based on converters' AH considering both the active and reactive power control. However, the effectiveness of the proposed model for power disturbances is not demonstrated, and the priority of the power-sharing is given for reactive power support. In [27], a fuzzy logic inference controller has been proposed to adapt the droop gains based on the converters' available power margin. In [28], based on the work of [25] and [27], the authors emphasized the importance of limiting the DC voltage deviation in addition to achieving the power-sharing based on the converters' local AH. An adaptive droop control has been presented with a factor that accounts for DC voltage deviations, considering the trade-off between DC voltage limits and power-sharing based on converters' available capacity. A different adaptive droop gain control has been presented in [29], with communication requirements among the AC grid-connected VSCs. This approach considered the frequency deviation of the AC grids, converters' AH, and the DC grid voltage deviation. However, based on the presented results, the droop gains are updated only one time, that is, at the start of the supply power variation. Therefore, in this work, consecutive power disturbances or Multi-Updated (MU) droop gains were not elucidated. Also, a similar frequency support approach to the previous work with adaptive droop control is presented in [31]. In [32], a continuous power-voltage characteristic parameterization has been introduced that can emulate the adaptive DC voltage droop control behavior in an MTDC system based on user-defined constraints (i.e., indirect adaptive DC voltage droop control). However, the presented approach does not consider the power-sharing based on the AH of the converters.

The previous works on the adaptive droop gain design for AH power-sharing have lacked the demonstration of the design approach during consecutive power disturbances. However, it is expected that due to input power fluctuations, the adaptive droop gain will have continuous adjustments based on the network's operating condition. It is of high importance to verify that the presented design approach is applicable for consecutive power disturbances during normal network operation, due to output variations of renewable energy sources. This paper investigates the effectiveness of previously-presented AH adaptive droop gain approaches in [25] and [29], which has shown DC network constraint violation during consecutive power disturbances. In addition, this paper presents another approach that can achieve power-sharing based on the converters' AH or loading capacity while complying with the network's constraints. An illustration of the paper's contribution is presented in Fig. 1.

The main aim of this paper is to present a comprehensive design approach for a decentralized adaptive DC voltage control in MTDC networks with a focus on the steady-state operation. This approach is applicable to small- and large-scale power disturbances, considering both converters' AH and loading capabilities while being constrained to the grid code. The impact of Single-Updated (SU), MU, and Irregular-Updated (IU) droop constant modification for consecutive power disturbances is evaluated. The previous works have lacked elaboration on the significance of the initial droop gains selection, which is highlighted in this paper. Moreover, a modified droop gain design is introduced to

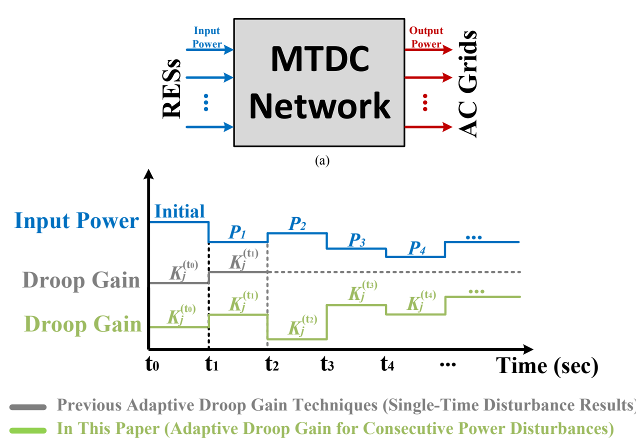

Fig. 1. An illustration of the paper's contribution (a) simplified representation of an MTDC network (b) simplified adaptive droop gain behavior with consecutive power disturbances, where P_i is the i^{th} power disturbance from the Renewable Energy Sources (RESs), $K_j^{(t_i)}$ is the droop gain during the i^{th} power disturbance, t_i is the i^{th} time of the occurrence of the power disturbance in RESs.

that in [25] and [29] for power-sharing based on the converter's AH and Loading Factor (LF) during consecutive power variations in an MTDC network. This considers stable post-contingency operation based on the converters' capabilities and the system's DC voltage limits.

The contributions of this paper can be summarized as follows.

- Evaluating the impact of initial droop gains adjustment and SU droop gains on an MTDC network during consecutive power generation variations.
- Investigating comprehensive system constraints for adaptive DC voltage droop control in MTDC systems during small- and large-scale power disturbances.
- Develop a decentralized approach for contingency versatile DC voltage droop control intended for a grid-side VSC with LF-based Droop (LFD) control and AH-based Droop (AHD) control considering converters' local and global LF and AH.
- Present case studies for AHD and LFD control with single-update, multi-update, and irregular-update of droop gains under MTDC network's power disturbances.

The structure of the paper is as follows. Section 2 delivers the background and problem definition of the adaptive DC voltage droop control in MTDC networks. Section 3 presents the design approach for LFD and AHD control. Section 4 elaborates on the presented concepts with case studies. Finally, Section 5 provides a summary of the work.

2. Background and problem definition

In this section, a brief background of MTDC system control and modeling is presented. Also, adaptive voltage droop control approaches are discussed.

2.1. MTDC system control and modeling

An MTDC network, shown in Fig. 2, may include several power input terminals, via Wind-Side Converters (WSCs), and power output terminals, via Grid-Side Converters (GSCs), with different possible HVDC interconnection topologies (e.g., radial and mesh) [33].

In general, the VSCs may act in constant power, constant DC voltage or DC voltage droop control modes through a combination of an outer control loop, as presented in (1), and inner control loop, as presented in (2) [34,35].

$$\gamma(V_{DC}{}^{*} - V_{DC}) + \mu(P_{DC}{}^{*} - P_{DC}) = 0 \tag{1}$$

where $\gamma = 0$ for constant power control mode, $\mu = 0$ for constant DC voltage control mode, and $\gamma \neq 0$, $\mu \neq 0$, for droop control mode. V_{DC} and P_{DC} are the measured voltage and power at the DC-side of the VSC, respectively. $V_{DC}{}^{*}$ and $P_{DC}{}^{*}$ are the reference set-points.

$$\begin{bmatrix} v_{t,d}{}^{*} \\ v_{t,q}{}^{*} \end{bmatrix} = \begin{bmatrix} u_{t,d} \\ u_{t,q} \end{bmatrix} + \omega L_T \begin{bmatrix} -i_q \\ i_d \end{bmatrix} + \begin{bmatrix} v_d \\ v_q \end{bmatrix} \tag{2}$$

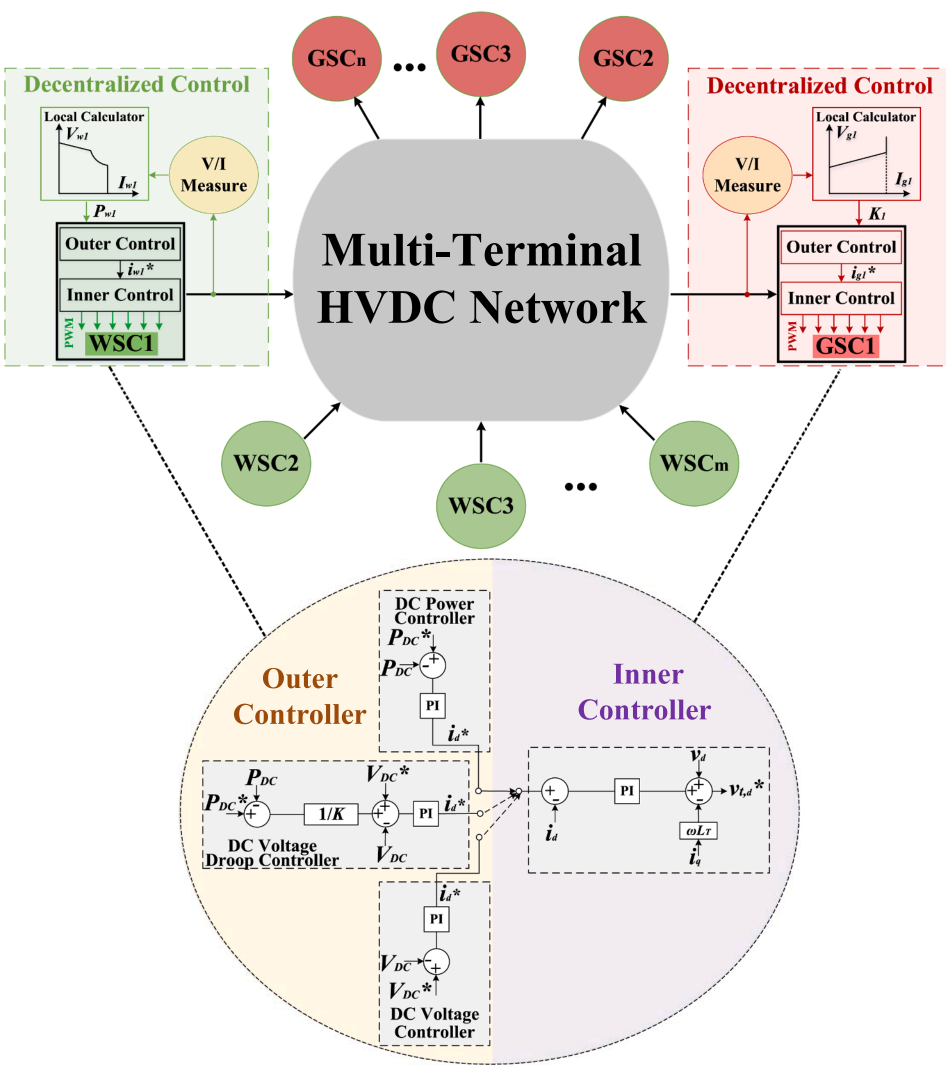

Fig. 2. General structure of decentralized control in an MTDC network (DC-side) with *m* WSCs and *n* GSCs.

where $v_{t,d}{}^*$ and $v_{t,q}{}^*$ are the internal control output voltages of the VSC in dq frame. $u_{t,d}$ and $u_{t,q}$ are the proportional-integral control signals for currents i_d and i_q. Such that $u_{t,d} = \left(k_{p,d} + \frac{k_{i,d}}{s}\right)(i_d{}^* - i_d)$ and $u_{t,q} = \left(k_{p,q} + \frac{k_{i,q}}{s}\right)(i_q{}^* - i_q)$. $k_{p,d}$, $k_{p,q}$ and $k_{i,d}$, $k_{i,q}$ are the proportional and integral gains, respectively. v_d and v_q are the VSC AC-side measured voltages in dq frame. ω is the angular frequency of the AC grid. L_T is the line reactor filter.

However, for balanced power flow in an MTDC system, during steady-state operation, the WSCs typically act in constant power control mode while the GSCs act in DC voltage droop control mode through voltage/current characteristic curves, as shown in Fig. 2 [36].

In this paper, the modeling of the MTDC system is based on the Average-Value Model (AVM) of the VSC, as presented in (3), [37–39], vector control for independent power control, as presented in (4), and π-equivalent DC circuit for the transmission line, as presented in Fig. 3 [10].

$$I_{DC} = \frac{2}{3}\frac{P_{DC}}{V_{DC}} \sum_{p=a,b,c} \left(\frac{2}{V_{DC}} v_{t,p}{}^*\right)^2 \tag{3}$$

where I_{DC} is the DC-side current flow of the VSC. p is an index that represents the AC-side phases.

Considering $P_{AC} = P_{DC}$ (i.e., lossless VSC), then the active and reactive power of the VSC are shown in (4) while considering the d-axis voltage is aligned with phase a of the grid voltage.

$$P_{DC} = v_d i_d \text{ and } Q = -v_d i_q \tag{4}$$

For a droop-controlled radial MTDC network with m WSCs and n GSCs, shown in Figs. 2 and 3, the system's load flow consists of a combination of $n + m + 2$ simultaneous nonlinear equations, as shown in (5)-(8).

$$\sum_{i=1}^{m} \frac{P_{wi}}{V_{wi}} = \sum_{j=1}^{n} \frac{V_r - V_{gL}}{R_{gj} + K_j} \tag{5}$$

$$V_{gj} - V_{gL} = \frac{V_r - V_{gL}}{(R_{gj}/K_j) + 1} \quad \forall\, j = 1, \cdots, n \tag{6}$$

$$V_{wi} - V_s = R_{wi}\frac{P_{wi}}{V_{wi}} \quad \forall\, i = 1, \cdots, m \tag{7}$$

$$V_s - V_r = \sum_{j=1}^{n} \frac{V_r - V_{gL}}{(R_{gj} + K_j)/R_T} \tag{8}$$

where R_T is the transmission line resistance between the two nodes V_s and V_r of the radial network in Fig. 3.

For a stable and secure network operation, the DC load flow of the radial MTDC network is constrained as follows.

$$\boldsymbol{V_{min}} \le \boldsymbol{V_{DC}} \le \boldsymbol{V_{max}} \tag{9}$$

where $\boldsymbol{V_{DC}} = [V_{w1}, \cdots, V_{wm}, V_s, V_r, V_{g1}, \cdots, V_{gn}]^T$. $\boldsymbol{V_{min}} = \boldsymbol{V_{gL}} - (\rho_{DC}\boldsymbol{V_{gL}})$ and $\boldsymbol{V_{max}} = \boldsymbol{V_{gL}} + (\rho_{DC}\boldsymbol{V_{gL}})$. $\boldsymbol{V_{gL}} = V_{gL}[1, \cdots, 1]^T$ with size $(n \times 1)$. The DC voltage deviation coefficient, ρ_{DC}, is 5% for steady-state operation or 10% for dynamic operation [39].

$$-\boldsymbol{P_{max}} \le \boldsymbol{P_{DC}} \le \boldsymbol{P_{max}} \tag{10}$$

where $\boldsymbol{P_{DC}} = [P_{w1}, \cdots, P_{wm}, P_{g1}, \cdots, P_{gn}]^T$.

$$-\boldsymbol{I_{max}} \le \boldsymbol{I_{DC}} \le \boldsymbol{I_{max}} \tag{11}$$

where $\boldsymbol{I_{DC}} = [I_{w1}, \cdots, I_{wm}, I_T, I_{g1}, \cdots, I_{gn}]^T$.

$$\boldsymbol{K_{min}} \le \boldsymbol{K} \le \boldsymbol{K_{max}} \tag{12}$$

where $\boldsymbol{K} = [K_1, \cdots, K_n]^T$. $\boldsymbol{K_{max}}$ and $\boldsymbol{K_{min}}$ are constrained to the objective of the power-sharing among the GSCs, the network operating-point, and the above constraints (9)-(11). Further elaboration on this constraint, (12), will be delivered in the following sections.

In this paper, the small- and large-scale power generation variations from the WSCs can be classified based on the assumption presented in (13).

$$\begin{aligned} &P_{inj} \le 0.5P_{cp}\,(\text{small} - \text{scale power generation variation}) \\ &P_{inj} > 0.5P_{cp}\,(\text{large} - \text{scale power generation variation}) \end{aligned} \tag{13}$$

where P_{inj} is the total power injected by the WSCs. P_{cp} is the total power capacity of the DC network.

2.2. Adaptive droop control techniques

The operating point of the droop gains (Ks) may divert during normal or abnormal network operation, as shown in Fig. 4, as in the case of power injection increase/decrease or the case of converter/line outages.

Fixed Ks can sustain the stability of the network for a specific range of operation; otherwise, the system may experience severe voltage levels or power flow imbalance that may damage the MTDC network infrastructure. The power exchange of droop-controlled GSCs is proportional to their local DC voltage. Thus, DC power flow variations are inherently adjusted based on Ks values. Fixed droop constants do no guarantee averting overrating violation. To alleviate this issue, researches attempted to develop an adaptive droop control for multi-operating point purposes. An essential objective of the adaptive droop control design in MTDC networks is the AH of the VSCs (i.e., the difference between the converter rating and the present power-sharing capacity), as shown in (14).

$$\boldsymbol{AH} = \boldsymbol{P_{g,r}} - \boldsymbol{P_g} \tag{14}$$

where $\boldsymbol{AH} = [AH_1, \cdots, AH_n]^T$. AH_j is the available headroom of the j^{th} GSC. $\boldsymbol{P_{g,r}} = [P_{g1,r}, \cdots, P_{gn,r}]^T$ is the vector of the power rating of the GSCs. $\boldsymbol{P_g} = [P_{g1}, \cdots, P_{gn}]^T$ is the vector of the present power shared by the GSCs.

The power-sharing among the GSCs, with adaptive droop control, during consecutive power disturbances, can be based on the converters' global and/or local AH and LF, as described in Table 1.

Where the Loading Factor (LF) of a j^{th} GSC is equivalent to $\left(\frac{P_{gj}}{P_{gj,r}}\right) * 100\%$.

The power-sharing based on the global AH of the GSCs requires the following condition, as elaborated in Table 1.

$$\begin{aligned} &\text{If } AH_a{}^{(t-1)} > AH_b{}^{(t-1)} > \cdots > AH_n{}^{(t-1)} \\ &\quad \therefore \Delta P_{ga}{}^{(t)} > \Delta P_{gb}{}^{(t)} > \cdots > \Delta P_{gn}{}^{(t)} \\ &\text{and } \Delta K_a{}^{(t)} < \Delta K_b{}^{(t)} < \cdots < \Delta K_n{}^{(t)}\ \forall\, t \end{aligned} \tag{15}$$

where $\Delta P_{gj}{}^{(t)} = P_{gj}{}^{(t)} - P_{gj}{}^{(t-1)}$. $\Delta K_j{}^{(t)} = K_j{}^{(t)} - K_j{}^{(t-1)}$.

Based on the GSCs' AH, the Ks can be adjusted, without a control mode change, to allow converters that are already operating near their limits not to share larger power. Consequently, this alleviates overloading conditions. Although it is possible to switch the control mode of the overloaded GSC into constant power control mode; however, this results in the GSC losing its DC voltage control ability.

Previous studies proposed adaptive droop control for AH consideration based on an inversely proportional relationship between the

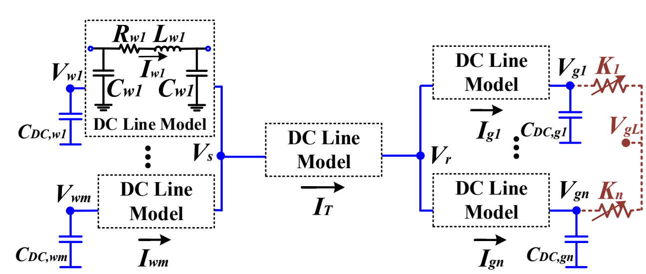

Fig. 3. DC equivalent circuit of a radial MTDC network, where $C_{DC,wi}$ and $C_{DC,gj}$ are the DC-link capacitor of the i^{th} WSC and j^{th} GSC, respectively.

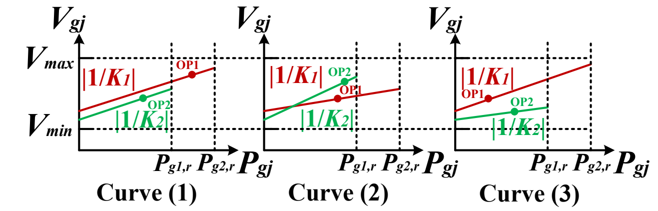

Fig. 4. Droop characteristic curves for two droop-controlled GSCs with different Operating-Points (OPs) and network conditions, where (Curve 1: $|K_1^{-1}|=|K_2^{-1}|$, Curve 2: $|K_1^{-1}|<|K_2^{-1}|$, Curve 3: $|K_1^{-1}|>|K_2^{-1}|$).

converter's AH and the converter's Ks, as shown in (16) with **Setting 1 ($\beta = 1$ and $\lambda = 1$)** [29] and **Setting 2 ($\beta = 0$ and $\lambda \neq 1$)** [25]. **Setting 1** compared to **Setting 2** in (16) requires additional parameters from neighbor GSCs, as shown in α, for the computation of the droop gains (i.e., **Setting 2** can obtain the droop gains with decentralized control action, while **Setting 1** requires communication among the GSCs).

$$K_j^{(t)} = K_j^{(t_0)}\alpha^{\beta}\left(\frac{MR^{[1-\beta]}\left(2P_{gj}{}^{(t-1)}\right)^{\beta}}{AH_j{}^{(t-1)}}\right)^{\lambda} \tag{16}$$

where $K_j^{(t_0)}$ is the initial K of the j^{th} GSC. t is the time at which the disturbance occurs. $\alpha = \frac{\sum_{s=1, s\neq j}^{n}\left(P_{gs,r}+P_{gs}{}^{(t-1)}\right)}{P_{gj,r}+P_{gj}{}^{(t-1)}}$. λ is a user-defined positive scaling factor (i.e., it is considered between 0.1 and 0.9, to avoid introducing substantial changes among Ks and the received power by the GSCs, during WSCs power injection variations). MR is the Maximum Power-Rating of the GSCs (i.e., $MR = \max(P_{gj,r})$).

Three types of droop gain behavior are presented in this paper: MU, SU, and IU droop gains (Ks), as shown in Fig. 5. The MU droop gains (Ks) are based on updating the droop constant at each time a system disturbance occurs. While for the SU droop gains (Ks) (an update for the first power variation directly after the initial condition), the time factor is neglected (i.e., $K_j^{(t+1)} = K_j^{(t)}\ \forall\ t$), as elaborated in Fig. 5. The IU droop gains (Ks) are based on updating the droop constants at non-regular disturbance time intervals based on specified criteria, as elaborated further in Section 3.3.

2.3. Evaluation of the adaptive droop control techniques

The impact of MU and SU droop gains in a 4-terminal radial network of 400 kV DC-link voltage, with two WSCs and two GSCs, is tested using (16) with both settings independently (Setting 1 [29] and Setting 2 [25]). The network data is presented in the appendix. The power delivered by the 1st WSC varies between 200 MW and 480 MW, while the power injection from the 2nd WSC is maintained constant at 300 MW, as shown in Fig. 6. The initial Ks for both GSCs are assumed 5 Ω. In addition, the Ks are adjusted to this value between 0 sec to 1 sec, while λ is assumed 0.4 for Setting 2. The disturbance time is considered at the incident of power variation, as shown in Fig. 6 (such that starting from t = 1sec). The DC voltages of the radial network are constrained

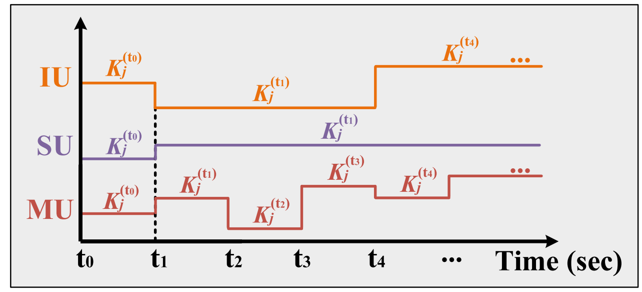

Fig. 5. Droop gains update behavior based on MU, SU, and IU.

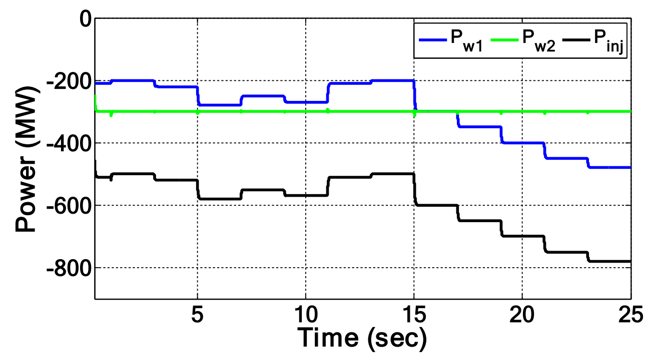

Fig. 6. Power injection variations from the WSCs, where P_{inj} is the total power injected to the radial MTDC network.

to ± 5% of the grid DC-link voltage. The droop gain values for the presented cases are available in the appendix.

In the case of consecutive power disturbances with:

Case 1 (MU Ks): in this case, the Ks are updated at each power disturbance. Based on Setting 1 in (16), and as shown in Fig. 7(a) and (c), $\Delta P_{g2}{}^{(t)} > \Delta P_{g1}{}^{(t)}$ (where $\Delta P_{gj}{}^{(t)} = P_{gj}{}^{(t)} - P_{gj}{}^{(t-1)}$) when $AH_2{}^{(t-1)} > AH_1{}^{(t-1)}\ \forall\ t$, and the reverse is true. This implies that the GSC with the highest AH takes more power during a disturbance. However, as shown in Fig. 7(a), even for a small-scale power injection/WSCs generation, around 50% of the system's total power capacity, (i.e., until t = 15 sec), the GSCs are having severe rating violation. While based on Setting 2 in (16), as shown in Fig. 8 (a) and (c), the power-sharing is not always based on the converters' global AH. Besides, power rating violation occurs during the large-scale power/WSCs power injection, around 80% of the system's total power capacity, which is after 21 sec.

Case 2 (SU Ks): in contrast to MU droop gains (Ks), the direction of the power fluctuation of GSCs in this case, $\Delta P_{gj}{}^{(t)}\ \forall\ j$, are unified. Based on Setting 1 in (16), the following behavior is attained: $|\Delta P_{g2}{}^{(t)}| > |\Delta P_{g1}{}^{(t)}|\ \forall\ t$, as shown in Fig. 7(b). This indicates that the GSC's power deviations follow the initial AH condition of the converter at t = 0 sec, that is $AH_2{}^{(t=0)} > AH_1{}^{(t=0)}$, as shown in Fig. 7(d). Although the AH behavior is reversed after the initial operating-point, $AH_1{}^{(t)} > AH_2{}^{(t)}$ $\forall\ t \neq 0$ sec. However, the changes on $P_{gj}\ \forall\ t$ are fixed to the initial

Table 1
Definition of power-sharing based on converters' global and/or local AH and LF for droop-controlled GSCs in MTDC systems.

Parameter	Definition	Equation
Global AH	The power-sharing among the GSCs during consecutive power disturbances is based on delivering more power to the converters with higher AH compared to the converters with lower AH (i.e., observing the behavior of all GSCs' AH to determine the power flow to the GSCs, for example, if GSCa AH is higher than GSCb AH at t_0, then at t_1 the GSCa shares more power compared to GSCb).	(15)
Local AH	During consecutive power disturbances, each GSC shares the power based on its AH, regardless of the other GSCs' AH (i.e., if a GSC AH is high at t_0, then at t_1 the GSC shares more power regardless of other GSCs' AH).	(17)
Global LF	The power-sharing among the GSCs during consecutive power disturbances is based on delivering more power to the converters with lower LF compared to the converters with higher LF (i.e., similar to Global AH; however, considering the converters' LF).	(26)
Local LF	During consecutive power disturbances, each GSC shares the power based on its LF, regardless of the other GSCs' LF (i.e., similar to local AH; however, considering the converters' LF).	(27)

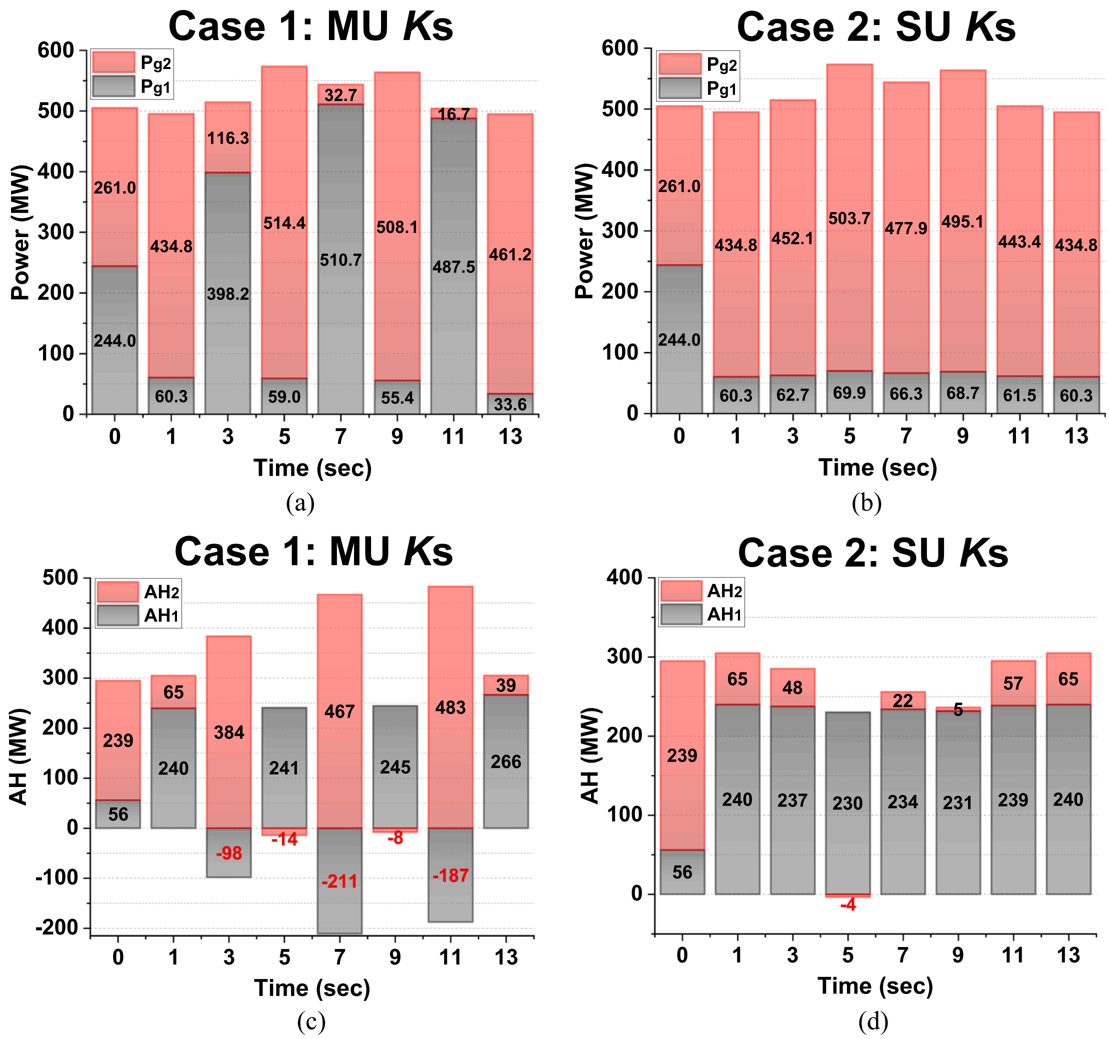

Fig. 7. The results of case 1 (MU *Ks*) and case 2 (SU *Ks*) for the 4-terminal radial MTDC network based on **Setting 1** in Eq. (16): (a) and (b) the power received by the GSCs, (c) and (d) the AH of the GSCs.

conditions. Thus, this case does not consider power-sharing based on the global AH of GSCs. Moreover, GSC rating violation is observed between 5 sec to 7 sec. While based on Setting 2 in (16), as shown in Fig. 8 (b) and (d), the following behavior is attained: $|\Delta P_{g2}{}^{(t)}| > |\Delta P_{g1}{}^{(t)}|$ and $AH_2{}^{(t)} > AH_1{}^{(t)}$ $\forall\, t$ until $t = 21$ sec. After that, the AH order is reversed (i.e., $AH_1 > AH_2$). However, the power changes of the GSCs do not follow the AH order. Thus, in this case, also, the power-sharing based on the converter's global AH is not guaranteed at all times, although no rating violation occurs.

Both settings in (16), with MU Ks, can achieve power-sharing based on the local AH of a GSC, that is achieving (17) as described in Table 1, yet with a system constraint violation. Besides, they do not consider the global AH, (15), and the burden introduced to other GSCs.

Based on the previous cases, the design of an adaptive droop control requires corrective actions to achieve the power-sharing based on the GSCs' global AH, while respecting the network's constraints, during a continuous disturbance in normal operation. In addition, corrective actions are required to eradicate the converter rating violation.

$$\begin{aligned}
&\text{If } AH_j{}^{(t-1)} > AH_j{}^{(t-2)} \\
&\therefore \Delta P_{gj}{}^{(t)} > \Delta P_{gj}{}^{(t-1)} \text{ and } K_j{}^{(t)} < K_j{}^{(t-1)} \quad \forall\, j\, \forall\, t \quad \text{or} \\
&\text{If } AH_j{}^{(t-1)} < AH_j{}^{(t-2)} \\
&\therefore \Delta P_{gj}{}^{(t)} < \Delta P_{gj}{}^{(t-1)} \text{ and } K_j{}^{(t)} > K_j{}^{(t-1)} \;\forall\, j\, \forall\, t
\end{aligned} \tag{17}$$

3. Modified adaptive DC voltage droop control: design approach

In this section, the essential constraints for adaptive droop control, in an MTDC network, are highlighted. Also, design approaches for adaptive droop control are presented, based on corrective actions, to avoid network constraints violation.

3.1. Design operational constraints

The adjustment of initial Ks, $K_j^{(t_0)}\ \forall\, j = 1, \cdots, n$, may impact the DC grid efficiency, voltage limits, and the behavior of the adaptive droop controller. Fig. 9 shows the terminal DC voltage of the 2nd WSC under the consecutive power variations presented in Fig. 6 (such that WSC2 terminal DC voltage is the highest voltage drop terminal across the network).

Meanwhile, tuning of Ks is based on the GSC's power rating, where the highest rated converter has a higher power-share contribution compared to the other converters $\forall\, t$ [29] (i.e., higher droop values are assigned to lower-rated converters), with SU droop gains, as shown in Table 2.

Three cases are considered for the adjustment of initial Ks, as shown in Table 2 and Fig. 9. The assumption of the initial Ks as $K_{ov}^{(t_0)} = 35\ \Omega$, optimal Ks with constraint violation, causes over-voltage in the MTDC grid. However, the initial Ks assumption as $K_{eff}^{(t_0)} = 25\ \Omega$, optimal Ks without constraint violation, rather than $K_{nv}^{(t_0)} = 5\ \Omega$, sub-optimal Ks,

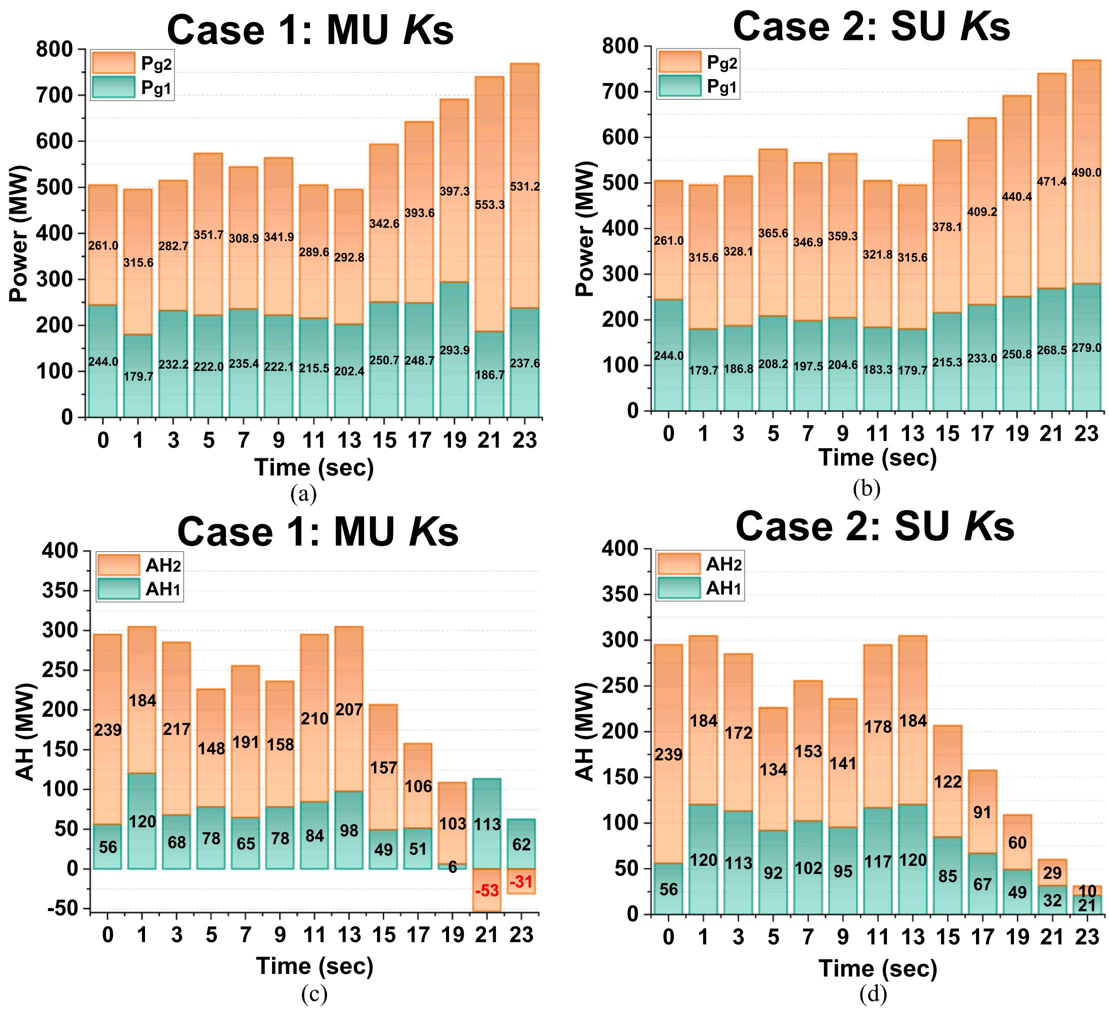

Fig. 8. The results of case 1 (MU *Ks*) and case 2 (SU *Ks*) for the 4-terminal radial MTDC network based on **Setting 2** in Eq. (16): (a) and (b) the power received by the GSCs, (c) and (d) the AH of the GSCs (larger power injection time-scale is considered here for Setting 2 in Eq. (16) compared to Fig. 7 to observe the possibility of power rating violation).

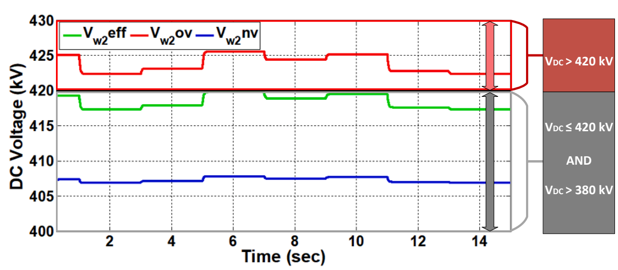

Fig. 9. DC voltage of WSC2 for the 4-terminal radial network, where $V_{w2}ov$, $V_{w2}nv$, and $V_{w2}eff$ are the voltages in case of **over-voltage** (i.e., optimal *Ks* with constraint violation), **normal-voltage** (i.e., sub-optimal *Ks*), and **efficient** (i.e., optimal *Ks* without constraint violation) network operation.

Table 2
4-Terminal radial network GSC's droop values and transmission losses.

Parameter		(Case 1) $K_{ov}^{(t_0)}$	(Case 2) $K_{nv}^{(t_0)}$	(Case 3) $K_{eff}^{(t_0)}$
Initial Droop Constant (Ω)		35	5	25
Droop Constant (Ω)	K_1	58.33	8.33	41.67
$\forall t > 1$ sec	K_2	21	3	15
Average Power Loss (MW)		4.996	5.398	5.124

results in higher transmission efficiency (i.e., allowing the system to operate near the maximum allowed DC voltage, 1.05 pu, or 420 kV, as shown in Fig. 9). That is while securing the network operation within its limits. As the initial Ks increases, then with its virtual resistance behavior, the GSCs share less power. Thus, the network DC voltage rises significantly (i.e., higher initial Ks results in lower transmission losses, as presented in Table 2). This shows that initial Ks selection requires careful consideration for any operating-point while optimizing the system efficiency and considering the voltage constraints.

For adaptive droop control, based on GSCs' global AH, in a radial MTDC network, it is essential to consider (9)–(11) in addition to (15), (18),(19), (22), and (23), for stable system operation.

$$0 \le AH_j^{(t)} \le P_{gj,r} \quad \forall\, t \tag{18}$$

$$K_1^{(t_0)} = K_2^{(t_0)} = \ldots = K_n^{(t_0)}$$
$$\text{for} \quad min\,[xP_{loss} + y\Delta V_{DC}] \tag{19}$$

where $\Delta V_{DC} = \sum_{i=1}^{k} |\Delta V_{DC,i}|$ for $k = n + m + 2$. $P_{loss} = \sum_{r=1}^{l} I_{DC,r}{}^2 R_{DC,r}$ for l transmission line with line resistance $R_{DC,r}$ and DC current $I_{DC,r}$. x and y are weighting factors.

For SU Ks, in the case of availability of forecasted wind generation data with high certainty level, the initial Ks can be based on the maximum, $P_{wi,max}$, and minimum, $P_{wi,min}$, power generation from the WSC with the highest line voltage drop, $max\,(I_{wi}R_{wi})$ with $V_{wi} = 1.05$ pu. This allows avoiding over/under voltage operation and maximizing the transmission efficiency with SU droop gain. While for MU Ks under consecutive power disturbances, a droop gain perturbation technique is essential to meet system constraints, as will be elaborated later.

Another critical aspect of the droop control design is the droop constant deviation, that is to what extent $K_j^{(t)}$ deviates from $K_j^{(t-1)}$. This deviation reflects on the alteration of the received power from $P_{gj}^{(t-1)}$ to $P_{gj}^{(t)}$. The substantial change from one operating-point to another, as in the case of Fig. 7(a), can cause frequency instability at the AC-side. Therefore, during power disturbances, it is recommended to apply a smooth transition function for Ks computation, to reduce the power fluctuation of the GSCs. As shown in (20) and (21), the variation on Ks can reflect directly on the GSC's power and voltages.

$$V_{gj}{}^{(t)} = V_{gL} + I_{gj}{}^{(t)}K_j{}^{(t)} \tag{20}$$

$$P_{gj}{}^{(t)} = I_{gj}{}^{(t)}V_{gj}{}^{(t)} \tag{21}$$

Thus, a scaling factor is required to control the shift of the Ks from one operating-point to another, as shown in (22).

$$|K_j^{(t-1)} - \varepsilon_j{}^{(t)}| \le K_j^{(t)} \le |K_j^{(t-1)} + \varepsilon_j{}^{(t)}| \quad \forall\, t \tag{22}$$

where ε_j is the scaling factor, restricted to realizing (9)–(11).

Moreover, for salient droop control action, the droop gain needs to be dominant over the respective line resistance, as shown in (23).

$$K_j{}^{(t)} > R_{gj} \;\forall\, j \;\forall\, t \tag{23}$$

Besides, the tendency, or the Probability (Pr), of a converter capacity violation, during consecutive power disturbances, increases with the proliferation of the deviation among Ks values, as shown in (24) for two GSCs with Ks K_a and K_b.

$$\begin{gathered}\text{If } \; K_a{}^{(t-1)} \gg K_b{}^{(t-1)} \therefore Pr(b)\uparrow \\ \{b|\; b = P_{gb}{}^{(t)}, \text{ where } \; P_{gb}{}^{(t)} > P_{gb,r}\}\end{gathered} \tag{24}$$

3.2. Modified Loading Factor-Based Droop (LFD) control

Employing Setting 1 in (16) without considering the previous design constraints may result in converter rating violation, randomized power-sharing action, and/or over/under voltage operation, due to the high scaling factor introduced to Ks, as shown in the appendix Fig. 23(a), through the time variations with MU Ks. In the case of power injection disturbances, the deployment of Setting 1 in (16) gives significant update actions on Ks values and on the received power by the GSCs. The capacity violation can be avoided by saturating the received power with a power limiter. However, this turns out to result in a repetitive constraint violation during the power disturbances. Also, in the case of MU droop gain, the power-sharing alternation among the GSCs remains large on the AC grids. To smooth the function in (16) considering Setting 1, an approximated form is obtained through Taylor's expansion, as shown in (25). The result of the expansion is elaborated in Fig. 10. The behavior of the functions in (16) and (25) for Setting 1 are compared in Fig. 10.

$$K_j{}^{(t)} = K_j^{(t_0)}\alpha^{\beta}\left(\frac{\mathrm{MR}}{P_{gj,r}}\right)^{\lambda.[1-\beta]} \sum_{\substack{k=0 \text{ for } \beta=0 \\ k=1 \text{ for } \beta=1}}^{3} 2^{\beta}\left(\frac{c_k}{b_k}\right)^{[1-\beta]} \frac{(P_{gj}{}^{(t-1)})^k}{P_{gj,r}{}^k} \tag{25}$$

where $\boldsymbol{c} = [c_0, c_1, c_2, c_3] = [1, \lambda, \lambda(\lambda+1), \lambda(\lambda^2+3\lambda+2)]$; $b_0 = 1$; and $b_k = k!$. $\boldsymbol{\beta} = 1$ **and** $\boldsymbol{\lambda} = 1$ **for Setting 1**.

Furthermore, a droop gain perturbation technique can be applied for tuning Ks at each operating-point, to achieve LFD control considering converters' global LF or AHD control considering converters' global AH, as will be elaborated in the following section.

In the case of expanding the 4-terminal radial MTDC network into a 5-terminal network, by employing an additional GSC, the functions (16) and (25) based in Setting 1 tends towards power-sharing based on the converter's loading capability. That is towards the LF, rather than the AH, as shown in (26) for global LF, while as shown in (27) for local LF, as described in Table 1. This allows decreasing the power-sharing among the loaded GSCs with priority given to highly loaded converters.

$$\begin{gathered}\text{If } \; LF_a{}^{(t-1)} > LF_b{}^{(t-1)} > \cdots > LF_n{}^{(t-1)} \\ \therefore \Delta P_{ga}{}^{(t)} < \Delta P_{gb}{}^{(t)} < \cdots < \Delta P_{gn}{}^{(t)} \;\forall\, t\end{gathered} \tag{26}$$

where $LF_j^{(t-1)} = P_{gj}{}^{(t-1)}/P_{gj,r}$.

$$\text{If } \; LF_j^{(t-1)} > LF_j^{(t-2)} \therefore \Delta P_{gj}{}^{(t)} < \Delta P_{gj}{}^{(t-1)}$$

or

$$\text{If } \; LF_j^{(t-1)} < LF_j^{(t-2)} \therefore \Delta P_{gj}{}^{(t)} > \Delta P_{gj}{}^{(t-1)} \;\forall\, j \;\forall\, t \tag{27}$$

The demonstration of the two functions in (16) and (25) based on Setting 1 for LFD control is presented in the results section.

3.3. Modified Available Headroom-Based Droop (AHD) control

The power-sharing based on Setting 2 in (16) can cause rating violations for the GSCs. In addition, the converter's global AH constraint in (15) is not met at all times. One way to achieve (15), while respecting network limits, is to update Ks in an irregular approach, IU Ks, as long as (28) is met. Rather than fixed Ks that can cause a burden on the GSC with the lowest K, Ks can be updated irregularly in the event of rating violation (28). This minimizes the action taken for Ks update and can guarantee (15).

$$\begin{gathered}\text{If } \; AH_a{}^{(t-1)} > AH_b{}^{(t-1)} > \cdots > AH_n{}^{(t-1)} \equiv AH_a{}^{(t-2)} > AH_b{}^{(t-2)} > \cdots \\ > AH_n{}^{(t-2)} \\ \therefore K_j^{(t)} = K_j^{(t-1)} \;\forall\, j\end{gathered} \tag{28}$$

That is to fix Ks based on Setting 2 in (16); however, if (28) is violated, then Ks shall be updated to continue achieving (15) $\forall\, t$. The selection of λ in (16) considering Setting 2 can reflect significantly on (22). In this paper, λ is considered between 0.1 and 0.9, to avoid introducing substantial changes among Ks and the received power by the GSCs, during power generation variations. In addition, to further allow

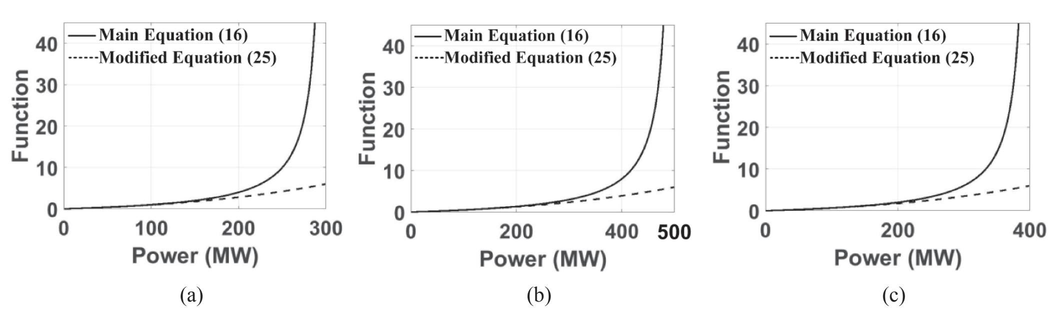

Fig. 10. LFD control function which is based on the main equation in (16) and the modified equation in (25) considering Setting 1, while employing: (a) GSC1 rating (b) GSC2 rating (c) and GSC3 rating (the ratings are available in the appendix).

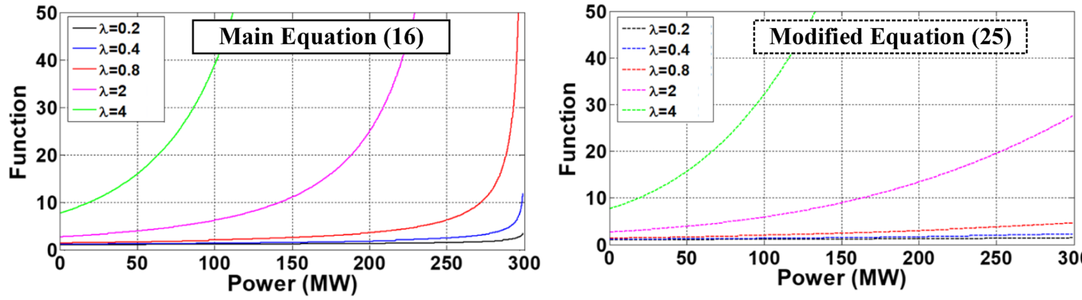

(a) (b)

Fig. 11. The effect of λ variations for the AHD control function based on Setting 2 in (a) the main equation in (16) and (b) the modified equation in (25) for GSC1 rating.

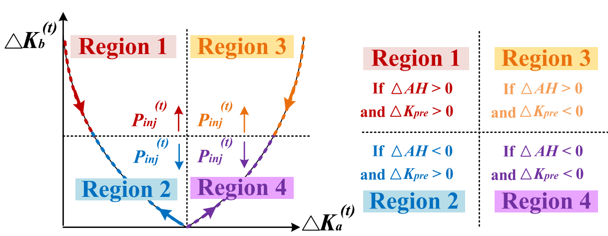

Fig. 12. Droop gain perturbation curve regions for two GSCs operation, GSCa and GSC$_b$, in case of WSCs power increase, P_{inj}↑, and decrease, P_{inj}↓, at time t, where $\Delta AH = AH_b^{(t-1)} - AH_a^{(t-1)}$, and $\Delta K_{pre} = \Delta K_{a,pre}^{(t)} - \Delta K_{b,pre}^{(t)}$.

a smooth gain transition, the insignificant elements of Setting 2 in (16) can be eliminated through Taylor's expansion, as shown in the modified function in (25) with $\beta = 0$ and $\lambda \neq 1$. The difference between the behavior of the two functions in (16) and (25) considering Setting 2, with several values of λ, is presented in Fig. 11.

3.4. Droop gain perturbation technique

For proper and stable power-sharing, during consecutive power disturbances with MU droop gain, based on the GSCs' global AH, Ks require perturbation and adjustment at each operating-point. The key point is to achieve (15) while respecting the network constraints. For adaptive droop control with droop gain perturbation technique, the perturbation term $\Delta K_j^{(t)}$ is introduced to achieve a power distribution based on the GSCs' global AH, as shown in (29).

$$K_j^{(t)} = \left(K_j^{(t_0)} \frac{MR}{P_{gj,r} - P_{gj}^{(t-1)}}\right)^{\lambda} + \Delta K_j^{(t)} \tag{29}$$

where $\Delta K_j^{(t)}$ is the perturbation variable. $MR = \max(P_{gj,r})$. $\lambda = 0.5$ for moderate Ks transition.

The first-term guarantees achieving power-sharing based on the GSC's local AH, that is, realizing (17). While the second-term is a perturbation variable to achieve power-sharing based on the global AH of the GSCs, that is achieving (15). The priority is given to the second-term, which is to reduce the power-sharing burden overall GSCs. The droop gain value at the previous time is referred to as $K_j^{(t-1)}$, while the droop gain value at the current time is referred to as $K_j^{(t)}$. The succeeding steps are followed to realize Ks perturbation for AHD control considering converters' global AH with two GSCs, GSCa and GSCb, (such that the same approach can be applied for n GSCs and for achieving the LFD control considering converters' global LF), around the operating-time $\forall\, j$, where $j \in (a, b)$.

1- Obtain the primary, pre-value, for Ks, $K_{j,pre}^{(t)}$ by (30).

$$K_{j,pre}^{(t)} = \left(K_j^{(t_0)} \frac{MR}{P_{gj,r} - P_{gj}^{(t-1)}}\right)^{0.5} \tag{30}$$

2- Calculate the primary perturbation value.

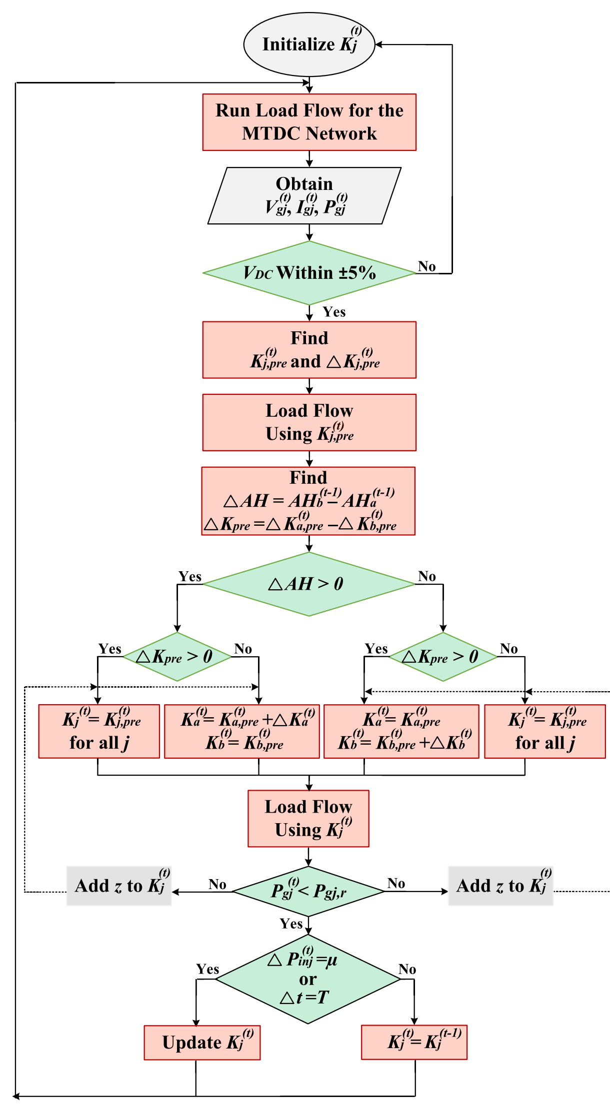

Fig. 13. Flowchart addressing droop gains perturbation for power-sharing based on global GSCs' AH.

$$\Delta K_{j,pre}^{(t)} = K_{j,pre}^{(t)} - K_j^{(t-1)} \tag{31}$$

3- Calculate the primary perturbation value between the two GSCs (such that this is in case $\Delta K_{b,pre}^{(t)} > \Delta K_{a,pre}^{(t)}$).

$$\Delta K_{ab}^{(t)} = \Delta K_{b,pre}^{(t)} - \Delta K_{a,pre}^{(t)} \tag{32}$$

4- Calculate the new perturbation value for the GSCa.

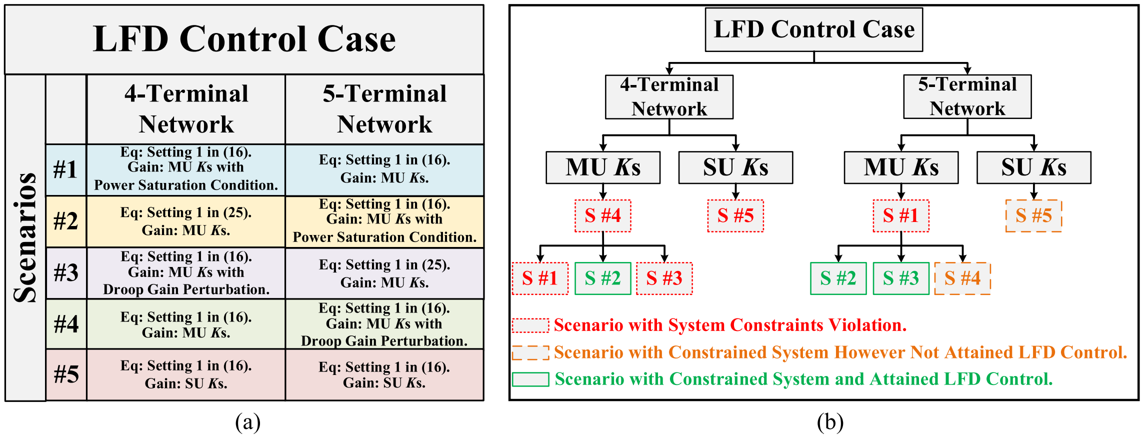

Fig. 14. Summary of the scenarios list for the LFD case study, where Eq refers to Equation, S # refers to scenario number, and scenarios #4 and #5 of the 4-terminal network refer to Case 1 and Case 2, respectively, in Section 2.3.

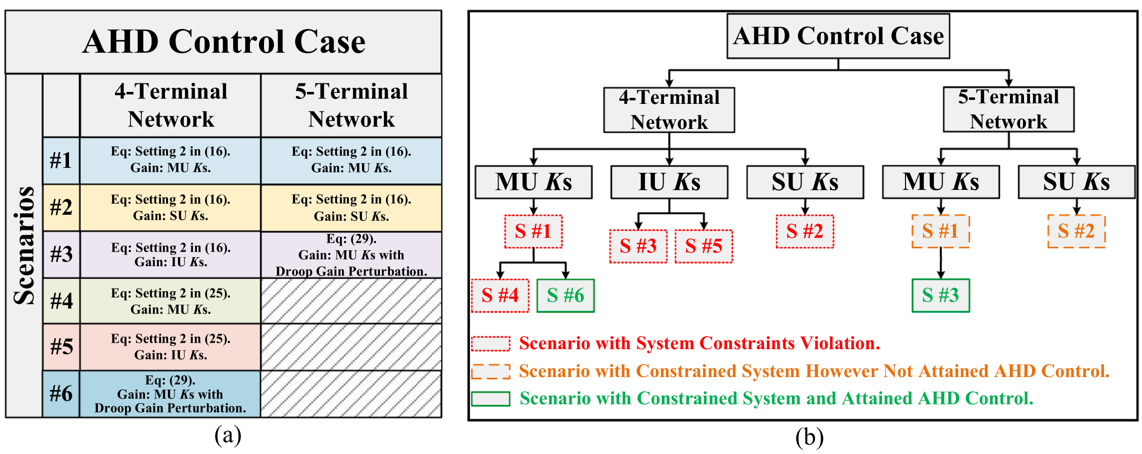

Fig. 15. Summary of the scenarios list for the AHD case study, where Eq refers to Equation, and S # refers to scenario number.

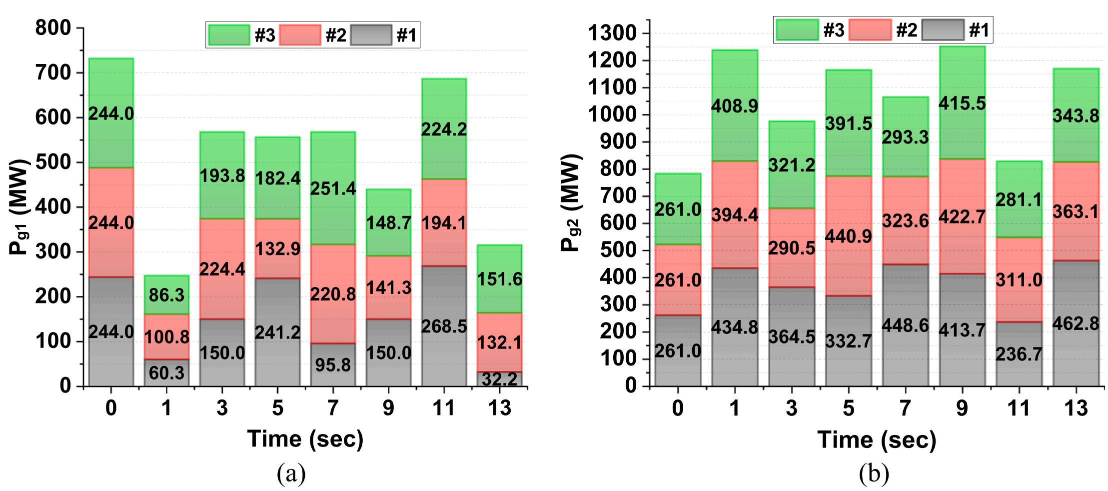

Fig. 16. 4-terminal radial network (a)-(b) power received by GSCs based on (#1) scenario 1, (#2) scenario 2, and (#3) scenario 3.

$$\Delta K_a^{(t)} = 2^{\alpha}\Delta K_{ab}^{(t)} \tag{33}$$

where α is assumed 0.5 to enlarge the perturbation among Ks to achieve power-sharing based on the GSCs' global AH.

5- In case of GSCs rating violation, then modify (33).

$$\Delta K_a^{(t)} = 2^{\alpha}\Delta K_{ab}^{(t)} + z \quad (\forall z \in \mathbb{R}) \tag{34}$$

where z can be a positive or negative number based on GSCs requirement, to avoid rating violation.

6- The final obtained Ks values at time t.

$$\begin{aligned} K_a^{(t)} &= \left(K_a^{(t_0)} \frac{MR}{P_{ga,r} - P_{ga}{}^{(t-1)}}\right)^{0.5} + \Delta K_a{}^{(t)} \\ K_b^{(t)} &= K_{b,pre}^{(t)} \end{aligned} \tag{35}$$

Figs. 12 and 13 give further elaboration about Ks perturbation

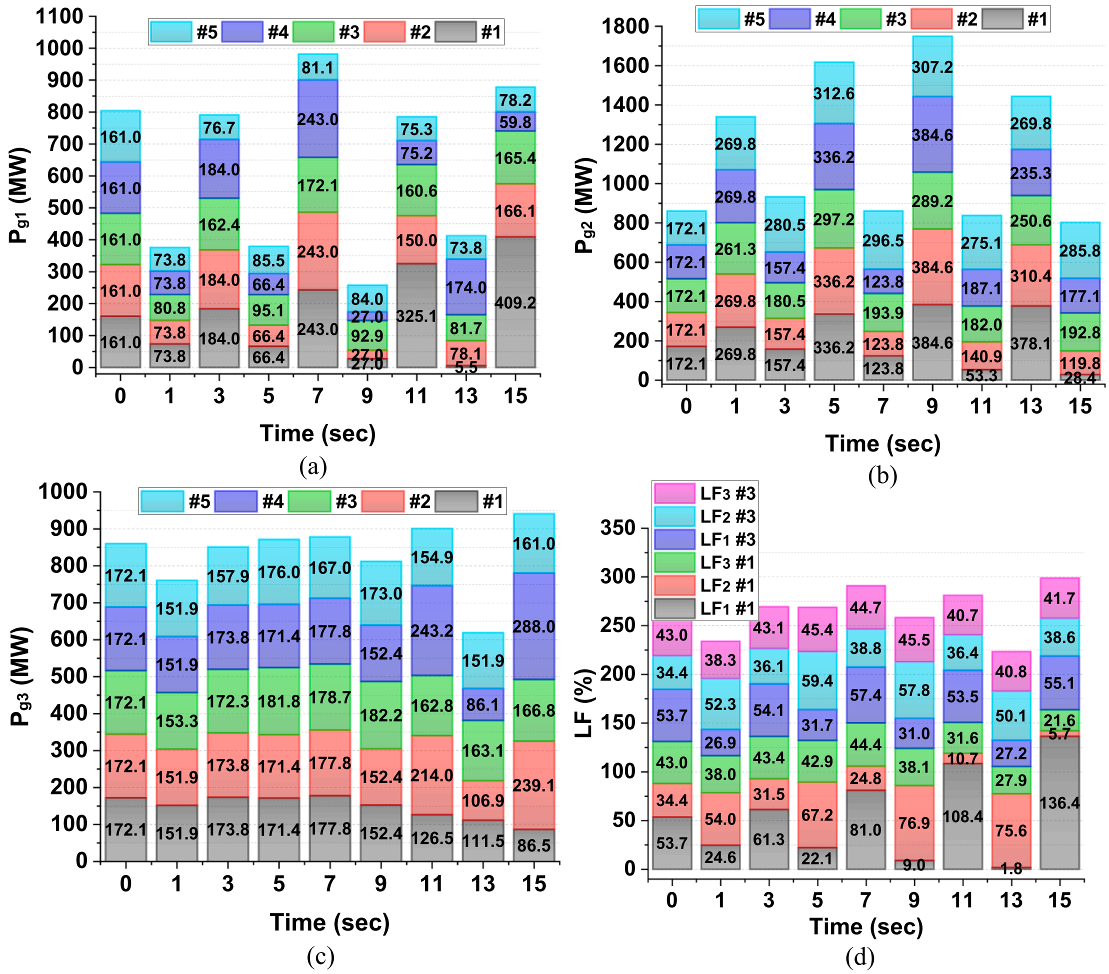

Fig. 17. 5-terminal radial network (a)-(b)-(c) power received by GSCs and (d) LF of the GSCs, based on (#1) scenario 1, (#2) scenario 2, (#3) scenario 3, (#4) scenario 4, and (#5) scenario 5.

Table 3
Operating condition status of the radial MTDC network for the LFD control case study.

Radial Network	Case 1 Scenario #	Achieving Droop Control Target: Local LF	Global LF	Local AH	Global AH	Constraints: V_{DC}	$P_{gj,r}$
4-Terminal	#1	✓	✓	✓	✓	✗	✓
	#2	✓	✓	✓	✓	✓	✓
	#3	✗	✗	✗	✗	✗	✓
	#4	✓	✓	✓	✓	✓	✗
	#5	✗	✗	✗	✗	✓	✗
5-Terminal	#1	✗	✓	✗	✗	✓	✗
	#2	✓	✓	✓	✗	✓	✓
	#3	✗	✓	✗	✗	✓	✓
	#4	✗	✗	✗	✗	✓	✓
	#5	✗	✗	✗	✗	✓	✓

The 4-terminal radial network scenarios #4 and #5 are the MU and SU Ks cases for Setting 1 in (16), respectively, in Section 2.3, as presented in Fig. 7. Where ✓ and ✗ means that local/global LF/AH objective and/or voltage & power constraints are either achieved or not achieved, respectively. The main objective of the table is to observe the cases that attain Global LF with no constraint violation for the DC voltage levels, V_{DC}, and the GSCs rating, $P_{gj,r}$.

technique. The flowchart in Fig. 13 starts by testing the fitness of the assigned initial Ks, such that in case the assigned initial Ks give a load flow within ± 5% of the DC-link voltage, then the droop gain perturbation function is calculated. After that, the DC network load flow is obtained by the droop gains generated from the droop gain perturbation function, and the GSCs' power constraints are checked. An additional check constraint that can be taken into consideration for Ks update, as introduced in the flowchart, is the frequency of the droop gain update. The system operator can control the update frequency based on the power change, ΔP_{inj}, or by imposing an update period, T,

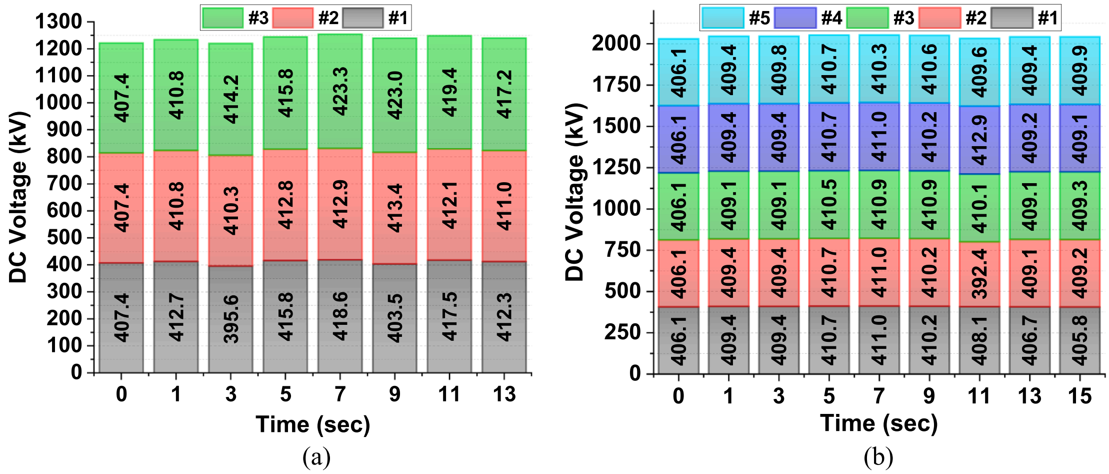

Fig. 18. The second WSC terminal DC voltage for the case study 1 different scenarios of (a) the 4-terminal network and (b) the 5-terminal network.

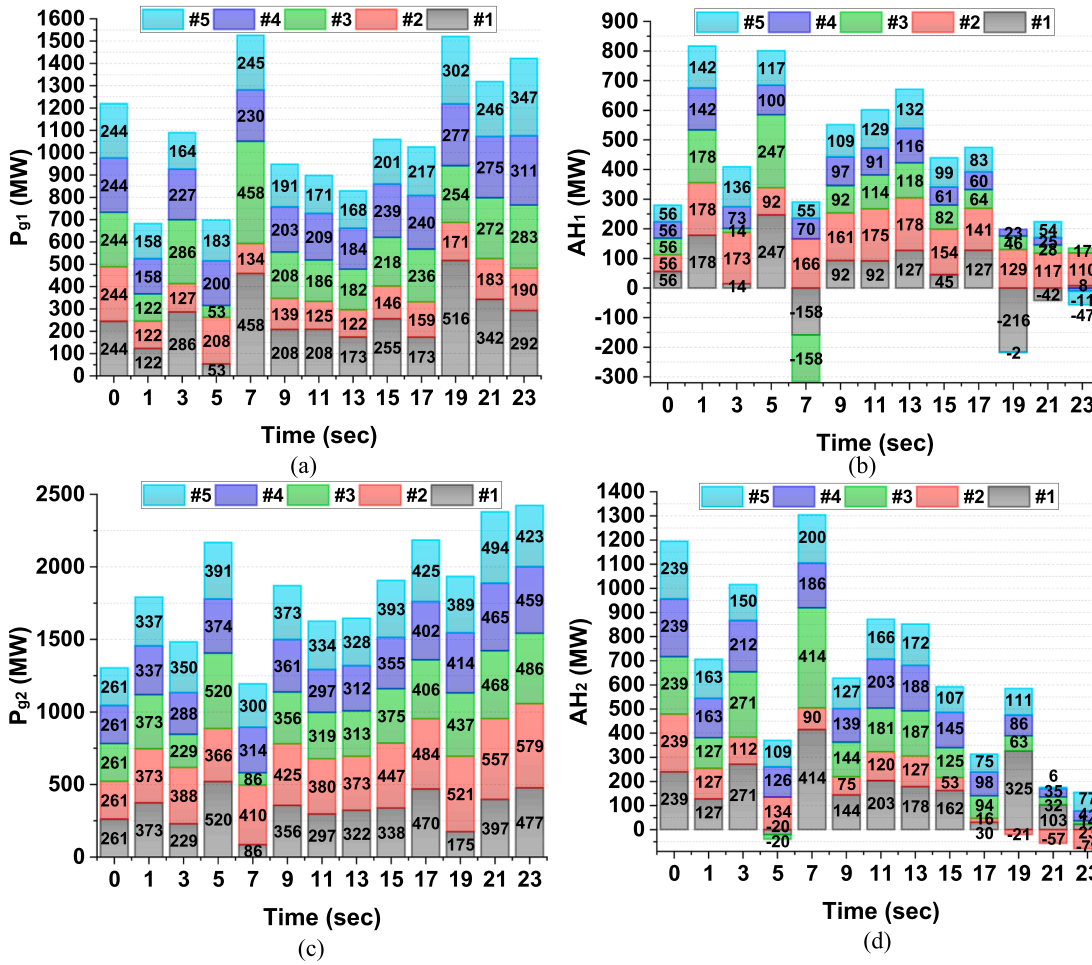

Fig. 19. 4-terminal radial network (a) and (c) power received by GSCs (b) and (d) AH of the GSCs based on (#1) scenario 1, (#2) scenario 2, (#3) scenario 3, (#4) scenario 4, and (#5) scenario 5.

to allow moderate Ks update frequency.

4. Case studies: approach verification

This section provides case studies for the presented concepts of LFD and AHD control, considering the radial MTDC network operation under both small-scale and large-scale power disturbances.

4.1. System modeling

The cases are presented using a 4-terminal radial network (i.e., with two GSCs) and a 5-terminal radial network (i.e., with three GSCs). The system data is available in the appendix. The power injection by the WSCs is presented in Fig. 6. The systems are implemented based on the AVM of the VSCs, as presented in Section 2.1. The initial Ks for the GSCs (i.e., in DC voltage droop control mode) are considered as $5\,\Omega$,

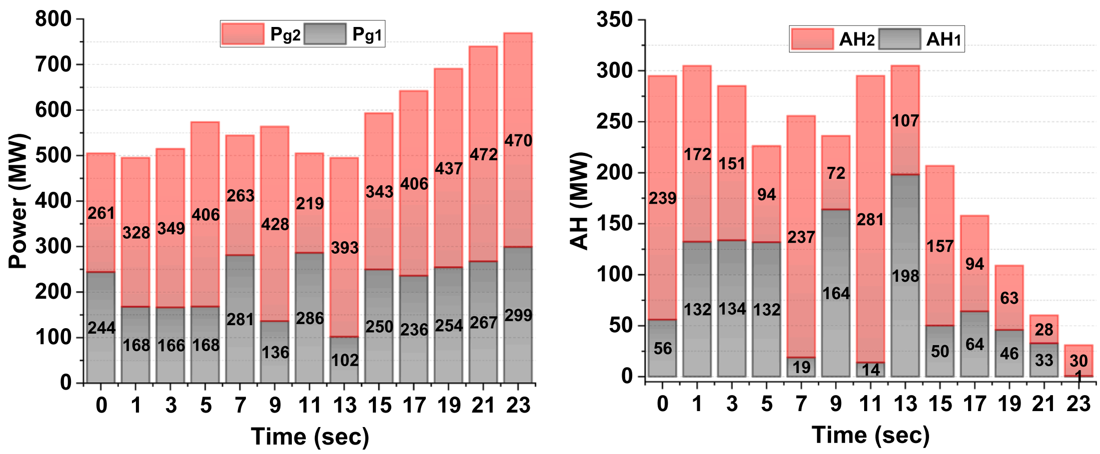

(a) (b)

Fig. 20. 4-terminal radial network scenario #6 (a) power received by GSCs and (b) AH of the GSCs based on *K*s perturbation technique.

which are applied for the operation period between 0 sec to 1 sec. The network DC voltage limit is targeted for ± 5% of the DC-link voltage, that is 380 kV $\leq V_{DC} \leq$ 420 kV.

A summary of the scenarios list considered for the LFD and AHD control case studies is presented in Figs. 14 and 15, while further details are presented in the following sections.

4.2. Case study 1: LFD control under consecutive power disturbances

Power-sharing based on LFD control in a radial network is investigated in this case with several scenarios and approaches. The different approaches are compared and are extracted from Setting 1 in (16) and (25), to share the power based on the GSCs' loading capability while being limited to the network's constraints for stable system operation.

The following are the scenarios considered for the 4-terminal network.

Scenario #1: the design of Ks is based on Setting 1 in (16) $\forall\ t$ with MU Ks. However, at the incidence of GSC rating violation at time $t-1$, then the design of Ks at t is based on a saturation condition, where for the violated GSC, its reference power is set to share 50% of its converter power rating.

Scenario #2: the design of Ks is based on Setting 1 in (25) with MU $Ks\ \forall\ t$.

Scenario #3: the design of Ks is based on Setting 1 in (16) with MU Ks. However, at the incidence of GSC rating violation at time $t-1$, then, at time t a droop gain perturbation factor is introduced to mitigate the change of $K_j^{(t)}$ from $K_j^{(t-1)}$ by half, that is to reduce $\varepsilon_j^{(t)}$ in compliance to (22) (i.e., $K_j^{(t)} = K_j^{(t-1)} + \frac{1}{2}(K_j^{(t)} - K_j^{(t-1)})\ \forall\ j$).

While the scenarios for the 5-terminal network are as follows.

Scenario #1: the design of Ks is based on Setting 1 in (16) $\forall\ t$ with MU Ks.

Scenarios #2, #3, and #4: the same as scenarios #1, #2, and #3, respectively, presented for the 4-terminal network.

Scenario #5: the design of Ks is based on Setting 1 in (16) with SU Ks (i.e., $K_1 = 31.2\ \Omega$, $K_2 = 8.1\ \Omega$, and $K_3 = 14.9\ \Omega\ \forall\ t > 1$ sec).

The results of these scenarios are presented in Figs. 16 and 17. Besides, the power-sharing status of the network is presented in Table 3.

The droop gain values for the main scenarios are presented in Fig. 24 in the appendix.

In the case of the 4-terminal network, **the first scenario** introduces a saturation limiter for the load flow in case the resultant droop gain results in a converter rating violation, as has been observed in Fig. 7(a). The limiter is activated for the 1st GSC, as shown in Fig. 16(a), at times 3 sec and 9 sec. However, this limiter imposes high droop gain value. Thus, the network DC voltages face a significant voltage drop at this operating duration, as shown in Fig. 18(a), where the 2nd WSC terminal is the node with the highest DC voltage drop across the grid. **The second scenario**, that is, the application of the modified function in (25) considering Setting 1, gives smooth GSC power change during the power variations, as shown in Fig. 16(a), compared to the application of Setting 1 in (16), as shown in Fig. 7(a). **In the third scenario**, at the incidence of GSC rating violation, which is initiated at $t = 3$ sec, the droop gain perturbation reduces the contribution of the converter power-sharing to alleviate constraint violation. Nonetheless, an overvoltage operation takes place between 7 sec and 11 sec, as shown in Fig. 18(a), due to improper adjustment of the perturbation factor. The first two scenarios mitigate violating the GSC rating while achieving the power-sharing based on the GSCs' loading availability or LF. Meanwhile, in the third scenario, the droop perturbation gain eliminates the converter power rating violation. However, the power-sharing is not preserved based on the GSCs' LF.

In the case of the 5-terminal network, **the first scenario**, that is, the application of the main function in (16) considering Setting 1, results in GSC1 power rating violation, as shown in Fig. 17(a). While introducing **scenarios 2 to 4**, to the 5-terminal network, for power rating violation eradication, appropriate power-sharing is achieved with stable system operation. Also, as can be seen in Fig. 17, the GSCs' power change during power injection variation is less imminent in scenarios 3 and 4. However, the fourth scenario gives priority to the converter rating constraint over achieving the LFD control, while the second and third scenarios give the power-sharing based on the LFD control considering converters' global LF. With SU Ks, **the fifth scenario**, the power-sharing of the GSCs is based on converters' initial LF throughout all the times. Thus, LFD control is not achieved.

According to the above scenarios, it can be concluded that for LFD control considering converters' global LF, the modified LFD method, Setting 1 in (25), gives a better power-sharing response among the GSCs while respecting the grid constraints during consecutive power disturbances.

4.3. Case study 2: AHD control under consecutive power disturbances

The following scenarios are considered for the AHD control case study in the 4-terminal network.

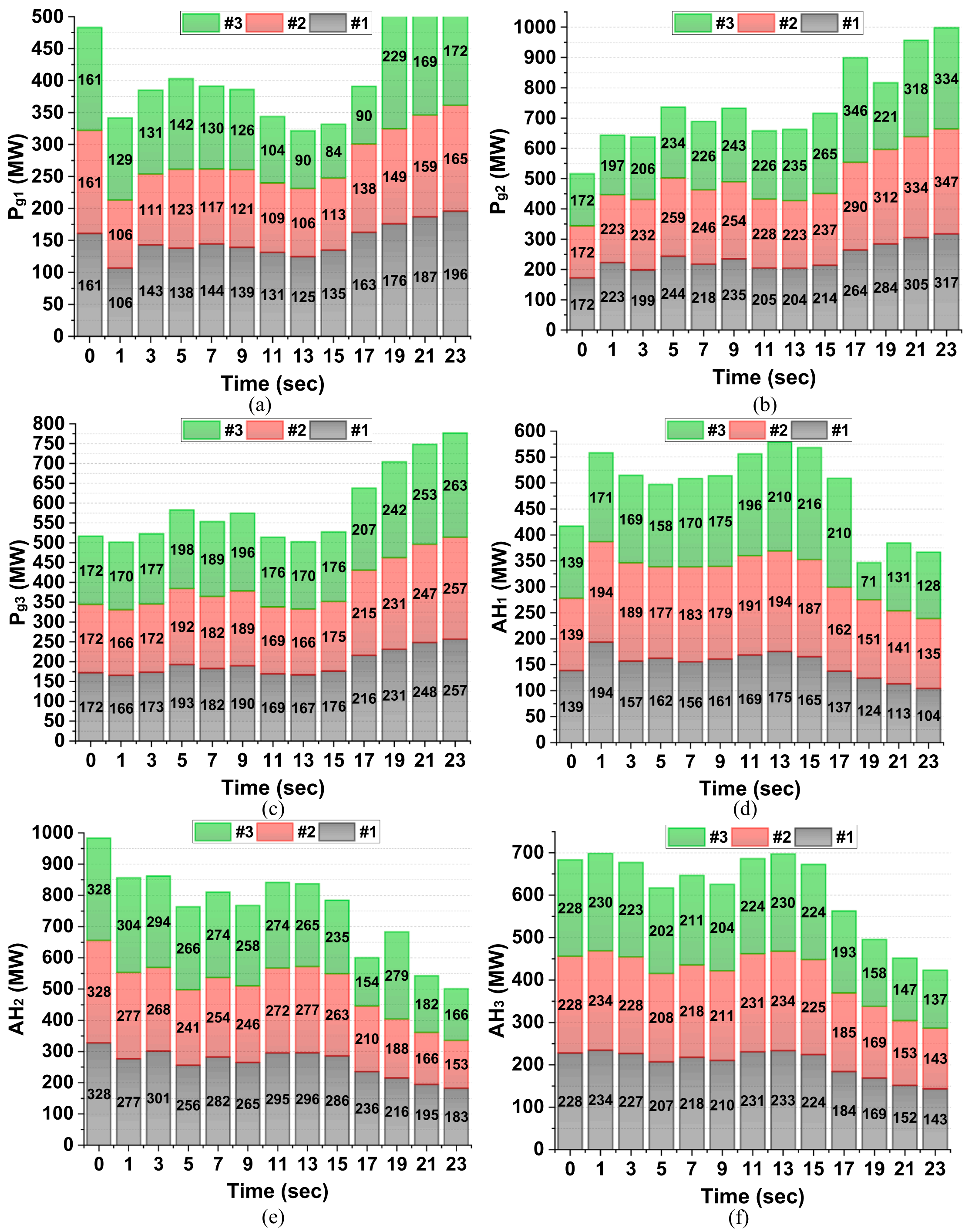

Fig. 21. 5-terminal radial network (a)-(b)-(c) power received by GSCs and (d)-(e)-(f) AH of the GSCs based on (#1) scenario 1, (#2) scenario 2, and (#3) scenario 3.

Scenario #1: the design of Ks is based on Setting 2 in (16) ∀ t with MU Ks.

Scenario #2: the design of Ks is based on Setting 2 in (16) with SU Ks (i.e., $K_1 = 28.8\ \Omega$ and $K_2 = 9\ \Omega$, ∀ $t > 1$ sec).

Scenario #3: the design of Ks is based on Setting 2 in (16) with IU Ks (i.e., Ks are updated whenever (15) is violated).

Scenario #4: the design of Ks is based on Setting 2 in (25) ∀ t with MU Ks.

Scenarios #5: the design of Ks is based on Setting 2 in (25) ∀ t with IU Ks (i.e., Ks are updated whenever (15) is violated), in this scenario, including the above scenarios, $\lambda = 0.8$.

Scenario #6: the design of Ks is based on the droop gain perturbation technique presented in Fig. 13.

The scenarios considered for the 5-terminal network are as follows.

Scenario #1 and #2: same as scenarios #1 and #2, consecutively, of the 4-terminal network. In these two scenarios, $\lambda = 0.9$. Where for Scenario #2, $K_1 = 15.8\ \Omega$, $K_2 = 7.3\ \Omega$, and $K_3 = 10.1\ \Omega$ ∀ $t > 1$ sec.

Scenario #3: same as scenario #6 of the 4-terminal network.

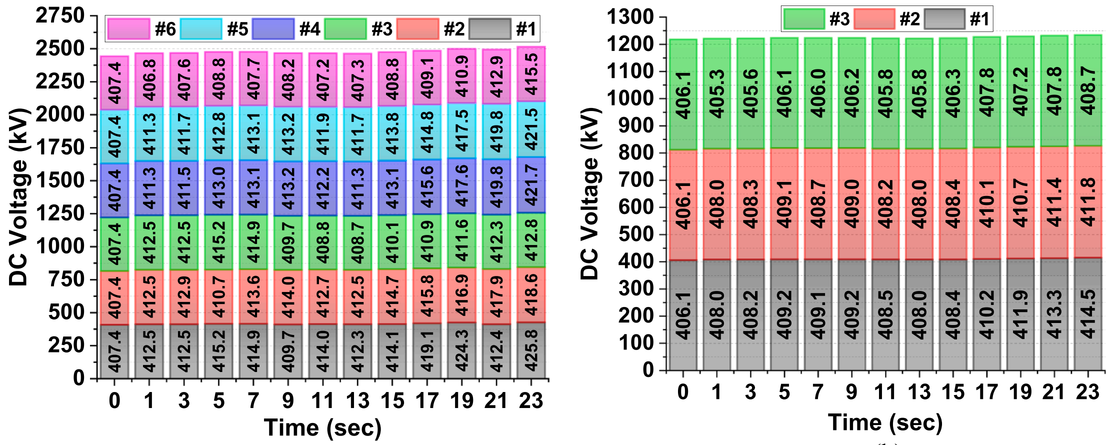

(a) (b)

Fig. 22. The second WSC terminal DC voltage for the case study 2 different scenarios of (a) the 4-terminal network and (b) the 5-terminal network.

Table 4
Operating condition status of the radial MTDC network for the AHD control case study.

Radial Network	Case 2 Scenario #	Achieving Droop Control Target: Local LF	Global LF	Local AH	Global AH	Constraints: V_{DC}	$P_{gj,r}$
4-Terminal	#1	✗	✓	✗	✗	✗	✗
	#2	✗	✗	✗	✗	✓	✗
	#3	✗	✗	✗	✓	✓	✗
	#4	✗	✓	✗	✗	✗	✗
	#5	✗	✗	✗	✓	✗	✗
	#6	✗	✗	✗	✓	✓	✓
5-Terminal	#1	✗	✗	✗	✗	✓	✓
	#2	✗	✗	✗	✗	✓	✓
	#3	✗	✗	✗	✓	✓	✓

Where ✓ and ✗ means that local/global LF/AH objective and/or voltage & power constraints are achieved or not achieved, respectively. The main objective of the table is to observe the cases that attain Global AH with no constraint violation for the DC voltage levels, V_{DC}, and the GSCs rating, $P_{gj,r}$.

Table 5
Assessment of the adaptive droop control techniques with MU droop gains.

Technique (Equation)	LFD (25) #1	LFD (16) #1	AHD/LFD (29)	AHD (25) #2	AHD (16) #2
Droop Control Objective	Reduce converters' LF.		Reduce converters' LF or utilize AH.	Utilize converters' AH.	
Objective Guaranteed	Yes	No	Yes	No	No
***K*s Variation**	Smooth	Sharp	Smooth	Smooth	Smooth
Communication Requirement	High	High	High	Low	Low
Constraints Met	Yes	No	Yes	No	No
Design Parameters' Number	High	High	High	Low	Low
Data Acquisition	Distributed Architecture			Decentralized Architecture	

Where #1 and #2 refer to Setting 1 and Setting 2, respectively, of Eqs. (25) and (16).

The results of the 4-terminal network scenarios are shown in Figs. 19, 20, 22, and Table 4. The droop gain values for the main scenarios are presented in the appendix Fig. 25.

In the case of the 4-terminal radial network, the application of the main function in (16) considering Setting 2, through **scenarios #1 to #3**, and the modified function in (25) considering Setting 2, in **scenarios #4 and #5**, do not guarantee, during wind-farms power variations, power-sharing within the converter power rating, as shown in Fig. 19 (a) and (c). The approach applied in scenario #5 can achieve AHD control with a smooth power-change transition, through IU *K*s. Nonetheless, in scenario #5, at large-scale power generation durations, the 1st GSC experience power rating violation. The AHD control considering converters' global AH can be achieved, within the network constraints, with the droop gain perturbation method, as presented by **scenario #6**, with moderate power-change transition among the GSCs, as shown in Fig. 20.

In the case of the 5-terminal radial network, the results of expanding the application of AHD control methods into a 5-terminal network with three GSCs are shown in Figs. 21, 22 and Table 4. The results with the main function in (16) considering Setting 2, presented in **scenarios #1 and #2**, does not achieve the AHD control, as shown in Fig. 21. However, it maintains the system within the constraints for stable operation. While in the case of Ks perturbation, **scenario #3**, the AHD control considering converters' global AH is achieved, within the allowed operational constraints, with moderate power-change among the GSCs at the incident of power disturbances, as shown in Fig. 21.

Table 5 presents an evaluation of the adaptive droop control techniques with respect to MU Ks.

The data acquisition structure of the droop control schemes presented in Table 5, distributed and decentralized architecture, depends on the communication-links among the GSCs [40]. Such that the decentralized structure requires solely local data acquisition for the droop gain design. Meanwhile, the distributed structure involves establishing communication-links among the GSCs for essential data exchange.

5. Conclusion

5.1. Paper goals and objectives

This paper presented generalized design approaches for adaptive DC voltage droop control in droop-controlled MTDC networks for power-sharing based on inverters' available headroom and loading capacity. The study focus was on renewable energy systems connected to AC grids through a high-power transmission DC grid system. The conventional available adaptive droop control methods were enhanced, and a droop gain perturbation technique was presented for proper power-sharing based on the AH and the LF of the converters. The impact of Multi-Updated (MU), Single-Updated (SU), and Irregular-Updated (IU) droop gains was explored through the deployment of different adaptive droop methods under consecutive power disturbances. Moreover, the vital operational constraints for stable system operation were presented to meet the power demand based on converters' and equipment's capabilities. Adaptive droop control can reduce the burden of power-sharing for the GSCs during the renewable energy supply fluctuations by the selection of a suitable droop gain. However, an inappropriate gain adjustment may jeopardize the stability of the system due to voltage limit and/or converter rating violation. The main objective of the paper was to present an approach for a contingency versatile DC voltage droop control with an adaptive droop gain based on the converter's AH or LF. Several approaches for the droop gain selection were tackled and simulated with 4-terminal and 5-terminal radial MTDC networks. The MTDC system modeling was based on the AVM of the VSC with Matlab/Simulink as the simulation platform. The presented approaches were evaluated in terms of achieving power-sharing based on local and global AH, and LF of the inverters.

5.2. Main outcomes

The paper covered the important aspects of the droop gain design from the steady-state perspective for constrained MTDC system operation, such as the initial adjustment of the droop gains, the droop constant deviation during consecutive power disturbances, and the salient droop control action. The adjustment of the initial droop gains can obtain optimal droop gains; however, with constraints violation (i.e., over-voltage operation as presented in Section 3.1). The proper tuning of the initial droop gains can compromise between the DC voltage deviation and system efficiency to achieve optimal power flow. For reduced droop constant deviation during consecutive power disturbances, a smooth droop gain computation function was advised and applied for the adaptive droop control techniques, as presented in Section 3.2 and Section 3.3. The salient droop control action was highlighted for the importance of the droop gains dominance over their respective DC lines resistances for prevailing control action. Moreover, the impact of SU droop gains was observed in Section 2.3 with a 4-terminal radial MTDC network, which demonstrated that it could cause converter limits violation. SU droop gains do not consider the converter's power rating nor capacity, therefore, adaptive droop gain approaches were advised with appropriate tuning for AH or LF power-sharing. While, for MU droop gain design (i.e., adaptive droop gain) during consecutive power disturbances, a droop gain perturbation technique was advised to provide a smooth function to avoid constraints violation.

The droop gain perturbation techniques were compared against the main existing adaptive droop gain techniques in the literature with a 4-terminal and 5-terminal radial MTDC network during consecutive power disturbances. The results showed that the droop gain perturbation method achieved the power-sharing based on the converters' AH while respecting the converter's power rating limits and the network's DC limits. Meanwhile, the other techniques, as shown in the results section and Table 5, do not guarantee achieving the power-sharing based on the converter's AH or LF, nor guarantee constrained network operation; except the smoothed modified function in (25) considering Setting 1 which achieved the power-sharing based on converter's LF with constrained network operation. While for example, the main function in (16) considering Setting 1 causes over-voltage operation, by 3 kV above 5% of the DC-link voltage, with the 4-terminal radial network scenario 3, as presented in Fig. 18 (a). In addition, the main function in (16) considering Setting 1 causes the GSCs to hit their power limits, as presented in case 1 in Section 2.3. A comparison between the used adaptive droop gain approaches and the advised droop gain perturbation technique was presented in Table 5, which supports the adequacy of the droop gain perturbation technique for power-sharing based on converters' capacity with constrained network operation and smooth droop gain transition during consecutive power disturbances.

Declaration of Competing Interest

The authors declared that there is no conflict of interest.

Acknowledgment

This publication was made possible by NPRP grant NPRP (9-092-2-045) from the Qatar National Research Fund (a member of Qatar Foundation). The statements made herein are solely the responsibility of the authors. Open Access funding provided by the Qatar National Library.

Appendix

See Figs. 23–25, and Table 6.

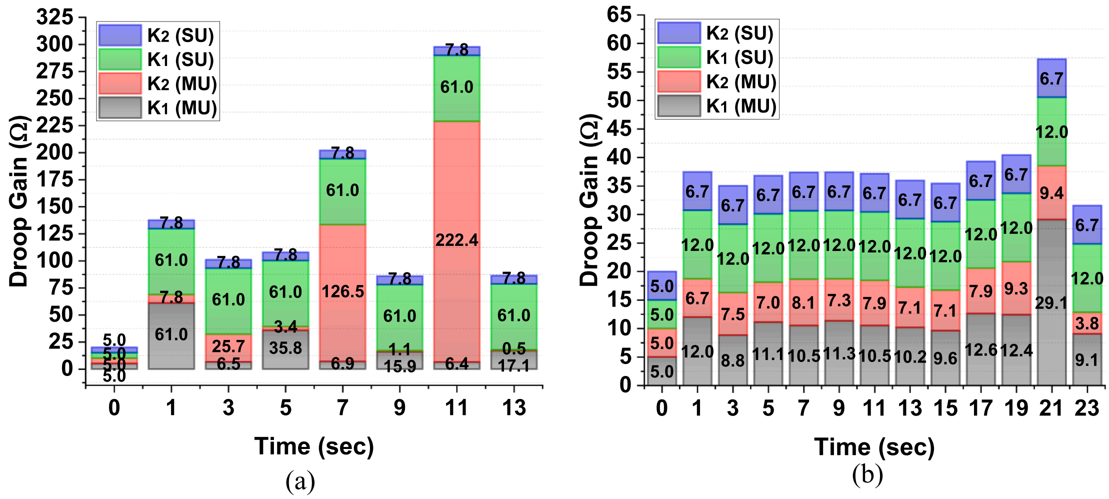

Fig. 23. Droop gain values for the case of (a) Setting 1 in (16) corresponding to Fig. 7, and (b) Setting 2 in (16) corresponding to Fig. 8.

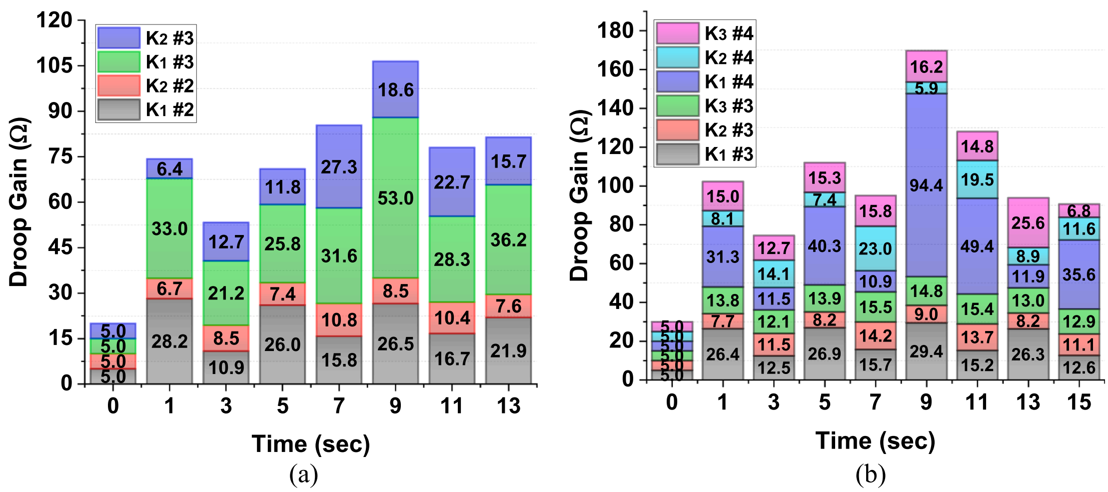

Fig. 24. Droop gain values for case study 1 (a) 4-terminal network scenarios #2 and #3 (b) 5-terminal network scenarios #3 and #4.

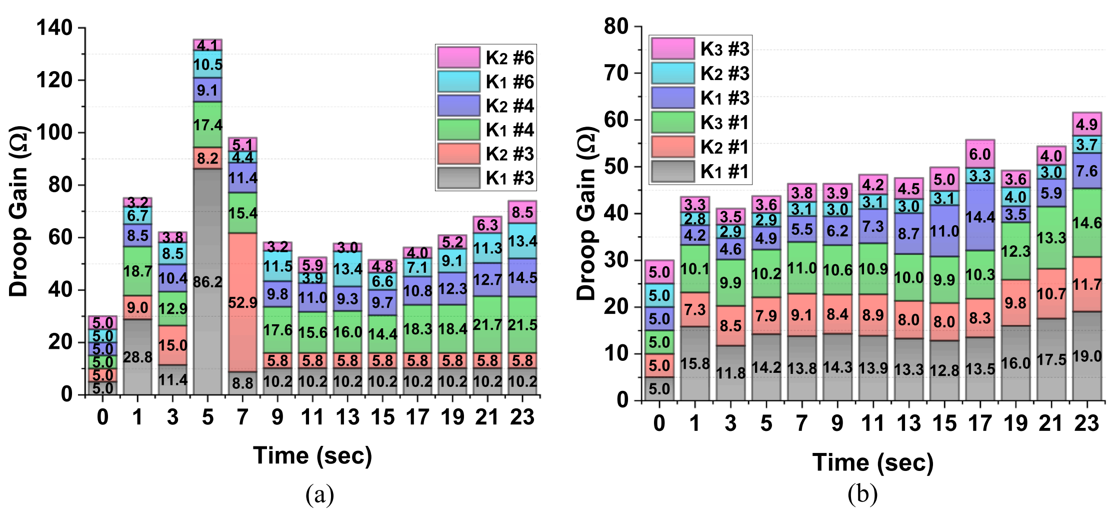

Fig. 25. Droop gain values for case study 2 (a) 4-terminal network scenarios #3, #4, and #6 (b) 5-terminal network scenarios #1 and #3.

Table 6
Radial MTDC testing network data and ratings based on Fig. 3.

Parameter	Value
Line Resistance (Ω)	$R_{w1} = 1$, $R_{w2} = 1.5$, $R_T = 2$, $R_{g1} = 1.2$,$R_{g2} = 0.8$
Line Inductance (mH)	$L_{w1} = 10$, $L_{w2} = 15$, $L_T = 40$,$L_{g1} = 12$,$L_{g2} = 8$
Line Capacitance (µF)	$C_{w1} = 11$,$C_{w2} = 16.5$,$C_T = 44$,$C_{g1} = 13.2$,$C_{g2} = 8.8$
DC-Link Capacitor (µF)	$C_{DC,wi} = 75$, $C_{DC,gj} = 75$
Converter Rating (MW)	$P_{w1,r} = P_{w2,r} = 500$, $P_{g1,r} = 300$,$P_{g2,r} = 500$,$P_{g3,r} = 400$
Line Rating (A)	2500
No-Load Voltage (kV)	400
Total System Capacity (MW)	1000

*The line data for the 3rd GSC is identical to the 2nd GSC.

References

[1] Meng K, et al. Hierarchical SCOPF considering wind energy integration through multiterminal VSC-HVDC grids. IEEE Trans Power Syst Nov. 2017;32(6):4211–21.
[2] Sinsel SR, Riemke RL, Hoffmann VH. Challenges and solution technologies for the integration of variable renewable energy sources—a review. Renewable Energy 2020;145:2271–85.
[3] Wen Y, Zhan J, Chung CY, Li W. Frequency stability enhancement of integrated AC/VSC-MTDC systems with massive infeed of offshore wind generation. IEEE Trans Power Syst Sept. 2018;33(5):5135–46.
[4] Rytoft C, Callavik M, Johansson H, Lundberg P, Jansson E, Bawa H, et al. ABB review special report 60 years of HVDC. Zurich: ABB Group R&D and Technology; 2014.
[5] Division EM. HVDC–high-voltage direct unrivaled practical experience. Erlangen: Siemens AG; 2017.
[6] Guelpa E, Bischi A, Verda V, Chertkov M, Lund H. Towards future infrastructures for sustainable multi-energy systems: a review. Energy 2019;184:2–21.
[7] Zhu J, Booth CD, Adam GP, Roscoe AJ. Coordinated direct current matching control strategy for multi-terminal DC transmission systems with integrated wind farms. Electr Power Syst Res 2015;124:55–64.
[8] Adeuyi OD, Cheah-Mane M, Liang J, Jenkins N. Fast frequency response from offshore multiterminal VSC–HVDC schemes. IEEE Trans Power Delivery Dec. 2017;32(6):2442–52.
[9] Kotur D, Stefanov P. Optimal power flow control in the system with offshore wind power plants connected to the MTDC network. Int J Electr Power Energy Syst 2019;105:142–50.
[10] Gavriluta C, Candela I, Luna A, Gomez-Exposito A, Rodriguez P. Hierarchical control of HV-MTDC systems with droop-based primary and OPF-based secondary. IEEE Trans Smart Grid May 2015;6(3):1502–10.
[11] Bianchi FD, Domínguez-García JL, Gomis-Bellmunt O. Control of multi-terminal HVDC networks towards wind power integration: A review. Renew Sustain Energy Rev 2016;55:1055–68.
[12] Li G, Du Z, Shen C, Yuan Z, Wu G. Coordinated design of droop control in MTDC grid based on model predictive control. IEEE Trans Power Syst May 2018;33(3):2816–28.
[13] Li X, Guo L, Hong C, Zhang Y, Li YW, Wang C. Hierarchical control of multiterminal DC grids for large-scale renewable energy integration. IEEE Trans Sustainable Energy July 2018;9(3):1448–57.
[14] Rouzbehi K, Miranian A, Luna A, Rodriguez P. DC voltage control and power sharing in multiterminal DC grids based on optimal DC power flow and voltage-droop strategy. IEEE J Emerging Selected Topics in Power Electron Dec. 2014;2(4):1171–80.
[15] Kirakosyan A, El-Saadany EF, Moursi MSE, Acharya S, Hosani KA. Control approach for the multi-terminal HVDC system for the accurate power sharing. IEEE Trans Power Syst July 2018;33(4):4323–34.
[16] Abdelwahed MA, El-Saadany EF. Power sharing control strategy of multiterminal VSC-HVDC transmission systems utilizing adaptive voltage droop. IEEE Trans Sustainable Energy April 2017;8(2):605–15.
[17] Sayed S, Massoud A. Minimum transmission power loss in multi-terminal HVDC systems: a general methodology for radial and mesh networks. Alexandria Eng J 2019;58(1):115–25.
[18] Aragüés-Peñalba M, Egea-Àlvarez A, Gomis-Bellmunt O, Sumper A. Optimum voltage control for loss minimization in HVDC multi-terminal transmission systems for large offshore wind farms. Electr Power Syst Res 2012;89:54–63.
[19] Aragüés-Peñalba M, Egea-Àlvarez A, Arellano SG, Gomis-Bellmunt O. Droop control for loss minimization in HVDC multi-terminal transmission systems for large offshore wind farms. Electr Power Syst Res 2014;112:48–55.
[20] Beerten J, Belmans R. Analysis of power sharing and voltage deviations in droop-controlled DC grids. IEEE Trans Power Syst Nov. 2013;28(4):4588–97.
[21] Xu L, Yao L, Bazargan M. DC grid management of a multi-terminal HVDC transmission system for large offshore wind farms. 2009 International Conference on Sustainable Power Generation and Supply, Nanjing, 2009, pp. 1-7.
[22] Abdel-Khalik AS, Massoud AM, Elserougi AA, Ahmed S. Optimum power transmission-based droop control design for multi-terminal HVDC of offshore wind farms. IEEE Trans Power Syst Aug. 2013;28(3):3401–9.
[23] Bianchi FD, Gomis-Bellmunt O. Droop control design for multi-terminal VSC-HVDC grids based on LMI optimization. 2011 50th IEEE conference on decision and control and European control conference, Orlando, FL; 2011. p. 4823–8.
[24] Sayed S, Massoud A. Impact of forced and unforced system parameter variations on network stability and system economics of radial MTDC networks. Electr Power Syst Res 2020;179. 106051.
[25] Chaudhuri NR, Chaudhuri B. Adaptive droop control for effective power sharing in multi-terminal DC (MTDC) grids. IEEE Trans Power Syst Feb. 2013;28(1):21–9.
[26] Li B, Liu T, Zhang Y. Unified adaptive droop control design based on dynamic reactive power limiter in VSC-MTDC. Electr Power Syst Res 2017;148:18–26.
[27] Chen X, Wang L, Sun H, Chen Y. Fuzzy logic based adaptive droop control in multiterminal HVDC for wind power integration. IEEE Trans Energy Convers Sept. 2017;32(3):1200–8.
[28] Wang Y, Wen W, Wang C, Liu H, Zhan X, Xiao X. Adaptive voltage droop method of multiterminal VSC-HVDC systems for DC voltage deviation and power sharing. IEEE Trans Power Delivery Feb. 2019;34(1):169–76.
[29] Yadav O, Kishor N, Negi R. Power imbalance sharing among the power converters in MTDC system. Int J Electr Power Energy Syst 2019;109:584–96.
[30] Yogarathinam A, Chaudhuri NR. Stability-constrained adaptive droop for power sharing in AC-MTDC grids. IEEE Trans Power Syst May 2019;34(3):1955–65.
[31] Wang W, Li Y, Cao Y, Häger U, Rehtanz C. Adaptive droop control of VSC-MTDC system for frequency support and power sharing. IEEE Trans Power Syst March 2018;33(2):1264–74.
[32] Marten A, Sass F, Westermann D. Continuous P-V-characteristic parameterization for multi-terminal HVDC systems. IEEE Trans Power Delivery Aug. 2017;32(4):1665–73.
[33] Gomis-Bellmunt O, Liang J, Ekanayake J, King R, Jenkins N. Topologies of multiterminal HVDC-VSC transmission for large offshore wind farms. Electr Power Syst Res 2011;81(2):271–81.
[34] Bahrani B, Kenzelmann S, Rufer A. Multivariable-PI-based *dq* current control of voltage source converters with superior axis decoupling capability. IEEE Trans Ind Electron July 2011;58(7):3016–26.
[35] Wu G, et al. Analysis and design of vector control for VSC-HVDC connected to weak grids. CSEE J Power Energy Syst June 2017;3(2):115–24.
[36] Gomis-Bellmunt O, Liang J, Ekanayake J, Jenkins N. Voltage–current characteristics of multiterminal HVDC-VSC for offshore wind farms. Electr Power Syst Res 2011;81(2):440–50.
[37] Weixing Lu, Ooi B-T. Optimal acquisition and aggregation of offshore wind power by multiterminal voltage-source HVDC. IEEE Trans Power Delivery Jan 2003;18(1):201–6.
[38] Sayed S, Massoud A. Optimal DC voltage control in multi-terminal HVDC network: modeling and scenarios. 2019 IEEE 9th symposium on computer applications & industrial electronics (ISCAIE), Malaysia, 2019. p. 86–91.
[39] Sayed S, Massoud A. A matlab/simulink-based average-value model of multi-terminal HVDC network. 2019 2nd international conference on smart grid and renewable energy (SGRE), Doha, Qatar; 2019. p. 1–6.
[40] Gavriluta C, Caire R, Gomez-Exposito A, Hadjsaid N. A distributed approach for OPF-based secondary control of MTDC systems. IEEE Trans Smart Grid July 2018;9(4):2843–51.